Tampereen yliopisto

Petteri Holkko

CHANGES IN CELL STRUCTURE AT THE PERIPHERY OF A MYOCARDIAL INFARCTION

Lääketieteen ja terveysteknologian tiedekunta
Syventävät opinnot
Joulukuu 2024

TIIVISTELMÄ

Petteri Holkko: Changes in cell structure at the periphery of a myocardial infarction
Lääketieteen lisensiaatin tutkinnon syventävät opinnot
Tampereen yliopisto
Lääketieteen lisensiaatin tutkinto
Joulukuu 2024

Sydän on elintärkeä lihaksikas elin, joka sijaitsee rintaontelossa. Sydän vastaa veren kuljettamisesta kehon kaikkiin elimiin. Yksi yleisimmistä sydänsairauksista on sepelvaltimotauti. Taudin edetessä sepelvaltimon luumen kaventuu, ja lopulta kliinisiä oireita ilmenee, kun sepelvaltimot ovat merkittävästi kaventuneet. Oireet voivat olla vakaa ja epävakaa angina pectoris, sydäninfarkti tai jopa äkkikuolema. Sepelvaltimotaudin johtaessa sydäninfarktiin, sydänlihas käy läpi dynaamisen uudelleenmuovautumisprosessin, jossa nekroottiset sydänlihassolut korvautuvat tiiviistä kollageenista muodostuvalla sidekudoksella. Aluetta, joka sydäninfarktin jälkeen ympäröi sidekudoksista ydintä, kutsutaan border zoneksi eli rajavyöhykkeeksi. Se on ohut kaistale selvinnyttä sydänlihasta, joka sijaitsee terveen sydänlihaksen ja sidekudoksisen alueen välissä. Border zone on hypokontraktiilia sydänlihaskudosta. Se saa normaalisti verisuonitusta, mutta siitä huolimatta se ei supistele kunnolla, ja tämän toimintahäiriön on havaittu pahenevan ajan myötä, kun uudelleenmuovautuminen etenee. Border zonen riski on kohonnut re-entry tyyppisille rytmihäiriöille. Tämä on suuri huolenaihe, sillä rytmihäiriökuolleisuus on korkea, eivätkä ne ole erityisen harvinaisia esimerkiksi sydäninfarktin yhteydessä.

Meidän tutkimuksessamme tarkastelimme happigradientin vaikutusta hiPSC-johdettuihin sydänlihassoluihin (hiPSC-CM). Erityisenä painopisteenä oli tumien kokojen ja sarkomeerirakenteiden muutokset. Käytimme tutkimuksessa erityistä happigradienttisirua, jossa hapen saturaatio toisessa päässä oli 0 % (hypoksia) ja toisessa päässä 19 % (normoksia). Happigradientin sirun keskialue jäljittelee border zonea akuutin sydäninfarktin aikana. Hypoksinen pääty jäljittele infarktoitunutta osaa sydämestä, missä ei ole verenkiertoa, ja normoksinen pääty simuloi tervettä, hyvin perfusoitua sydänlihasta. Ensimmäinen hypoteesimme oli, että happigradientissa hiPSC-CM:ien tumat ovat pienempiä kuin kontrollinäytteessä. Toinen hypoteesimme oli, että sarkomeerirakenteen muutoksia tai solurakenteen hajoamista olisi näkyvissä gradientissa. Kokeiden jälkeen emme havainneet merkittävää eroa, kun happigradientin tumia verrattiin normoksisiin, hypoksisiin ja kontrollinäytteen olosuhteisiin. Happigradienttiolosuhteissa tumien pituudet olivat noin 12.49 µm ja leveydeltään 6.45 µm. Happigradientti olosuhteissa sarkomeerien rakenne oli hyvin organisoitu, ja niissä oli selkeästi havaittavissa poikkijuovat. Yhteenvetona, happigradienttisirumme ei tuottanut muutoksia, jotka tiedetään esiintyvän border zonella in vivo, ja tämän vuoksi muutoksia tutkimusjärjestelyyn tarvitaan jatkossa.

Avainsanat: sydäninfarkti, border zone, gradientti, hiPSC-CM

TEKOÄLYN KÄYTTÖ OPINNÄYTTEESSÄ

Opinnäytteessäni on käytetty tekoälysovelluksia:

- ☐ Ei
- ☒ Kyllä

Ilmoitukseni mukaan olen käyttänyt opinnäytteessäni tutkielmaprosessin aikana seuraavia tekoälysovelluksia:

Tekoälysovellusten nimet ja versiot: Google Translate, ChatGPT 3.0 Free, and ChatGPT 3.5 Free.

Käyttötarkoitus: Tekstiä kirjoittaessa käytettiin Google Translatea käännöstarkoituksiin. Tekstin kirjoittamisen jälkeen ChatGPT:tä käytettiin tekstin oikolukemiseen, mikä tuotti kieliopillisesti parempaa tekstiä. Tieteelliseen kirjoittamiseen sopivia sanoja ja lauserakenteita kysyttiin ChatGPT:ltä, jos tarvitsin apua tekstin selkeyttämiseen. Ideat lisättiin tekstiin omin sanoin ilman kopiointia. Kaikkia Google Translaten ja ChatGPT:n antamia korjauksia tai ehdotuksia ei käytetty, jos niissä oli virheitä tai ne eivät olleet tarkoituksenmukaisia.

Osiot, joissa tekoälyä on käytetty: Tekoälyä käytettiin tekstin oikolukuun ja oikeinkirjoitusvirheiden korjaamiseen koko tekstissä. Tieteellisiä sanoja ja lauserakenteita koskevia ideoita pyydettiin tarvittaessa kirjallisuus- ja tulososioissa.

Olen tietoinen siitä, että olen täysin vastuussa koko opinnäytteeni sisällöstä, mukaan lukien osat, joissa on hyödynnetty tekoälyä, ja hyväksyn vastuun mahdollisista eettisten ohjeiden rikkomuksista.

Table of contents

1 Summary

The heart is a vital muscular organ. It is situated in the thoracic cavity, and its primary function is to supply oxygenated blood throughout the human body. (Tran et al., 2024.) One of the most common diseases related to the heart is coronary artery disease (CAD) (Álvarez-Álvarez et al., 2017). As the CAD progresses, vessel lumens narrow significantly, and eventually, clinical symptoms begin to manifest. It can manifest as stable and unstable angina, myocardial infarction, or sudden cardiac death. (Thygesen et al., 2012.) If CAD leads to myocardial infarction (MI), the heart undergoes a dynamic healing and remodeling process where necrotic cardiomyocytes are replaced by scar tissue with a dense collagen core (Arackal & Alsayouri, 2024). The area that surrounds this scar tissue is the border zone (BZ). It is a thin layer of surviving myocardium between the scarred and healthy heart tissue. (Mendonca Costa et al., 2018.) Despite receiving normal perfusion, the BZ fails to contract effectively, i.e., it is hypocontractile. This dysfunction worsens as the remodeling process progresses. (Jackson et al., 2002.) The BZ is known to have an increased risk for re-entry arrhythmias (Baumeister & Quinn, 2016), and it is a major concern because the mortality rate for arrhythmias is high, and they are not extremely rare, e.g., related to MI (Rymer et al., 2024).

In our study, we investigated if oxygen gradient impacts hiPSC-derived cardiomyocytes (hiPSC-CMs) structure. The focus was on changes in nuclei size and sarcomere structure. We employed a specialized oxygen gradient chip with oxygen levels ranging from 0 % saturation at one end to 19 % at the other. The middle of the gradient simulates the border zone during acute MI. The hypoxic end represents the infarcted region with no blood flow, and the normoxic end represents the healthy and well-perfused myocardium. We hypothesized that in an oxygen gradient, hiPSC-CMs' nuclei would be smaller compared to the control sample. The second hypothesis is that disruption of the sarcomere structure or destruction of cell structure would be present. However, we did not observe significant changes in nuclear size and sarcomere structure when comparing hiPSC-CMs from oxygen gradient to normoxic, hypoxic, and control conditions. The nucleus in the oxygen gradient was measured to be approximately 12.49 µm in length and 6.45 µm in width. Under gradient conditions, the sarcomeres displayed a highly organized, striated pattern, with distinct striations visible. In conclusion, our gradient chip would not reproduce abnormalities known to be present in this border zone in vivo, and thus, modification for the set-up is required.

2 Literature

2.1 Heart

The heart is a vital muscular organ whose main task is to supply blood for the whole human body and maintain sufficient perfusion to the vital organs. It is located between two lungs in the mediastinum, the middle part of the thorax cavity. The heart has four valves and four chambers. (Arackal & Alsayouri, 2024.) Two upper chambers are atrias and two lower two chambers are ventricles. Blood is pumped from the right side of the heart to the pulmonary circulation, and the left side pumps blood for the systemic circulation. Every chamber in the heart is divided by a mobile valve which controls the direction of the blood flow but also prevents blood's backflow. The muscular heart wall can be divided into three sections. The outer protective wall is called the epicardium, a thick middle part called the myocardium, which performs the contractile function of the heart, and a single-cell inner layer called the endocardium. (Tran et al., 2024.)

Two coronary arteries are located on heart's the epicardium layer, the left (LCA) and right (RCA). These provide the blood supply for the whole heart. The LCA is divided into two smaller arteries: the left anterior descending artery (LAD) and the left circumflex coronary artery (LCX). The LAD descends along the interventricular groove in the direction of the apex of the heart. It provides blood to the following parts of the heart: the anterior left ventricular myocardium, the two-thirds of the interventricular septum anteriorly, and the anterolateral papillary muscle, which is connected to the mitral valves. The other main artery, RCA, is located horizontally along the right atrioventricular groove. It ensures sufficient blood flow to the right ventricle, posteriorly for both ventricles and one-third of the posterior part of the interventricular septal myocardium and the posteromedial papillary muscle associated with the mitral valves. (Tran et al., 2024.)

2.2 Histology

Cardiomyocytes and connective tissue are the two main histological components of the heart. Cardiomyocytes are also known as cardiac muscle cells, which are unable to regenerate. These cells are able to contract under involuntary control. They are characterized by their striated appearances, branching structure, intercalated disks, and a large number of mitochondria. Cardiomyocyte typically contains one nucleus, and it is surrounded by a cell membrane. Voltage-gated calcium channels and various ion channels that are specialized for the myocyte's action

potential are located on the cell membrane. (Arackal & Alsayouri, 2024.) Contraction is executed by sarcomeres, which have two components: thin actin filament and thick myosin filament. Located between the cardiomyocytes are gap junctions (GJ), which connect cardiomyocytes. These cell-to-cell proteins allow quick spread of action potential in the myocardium. (Tran et al., 2024.)

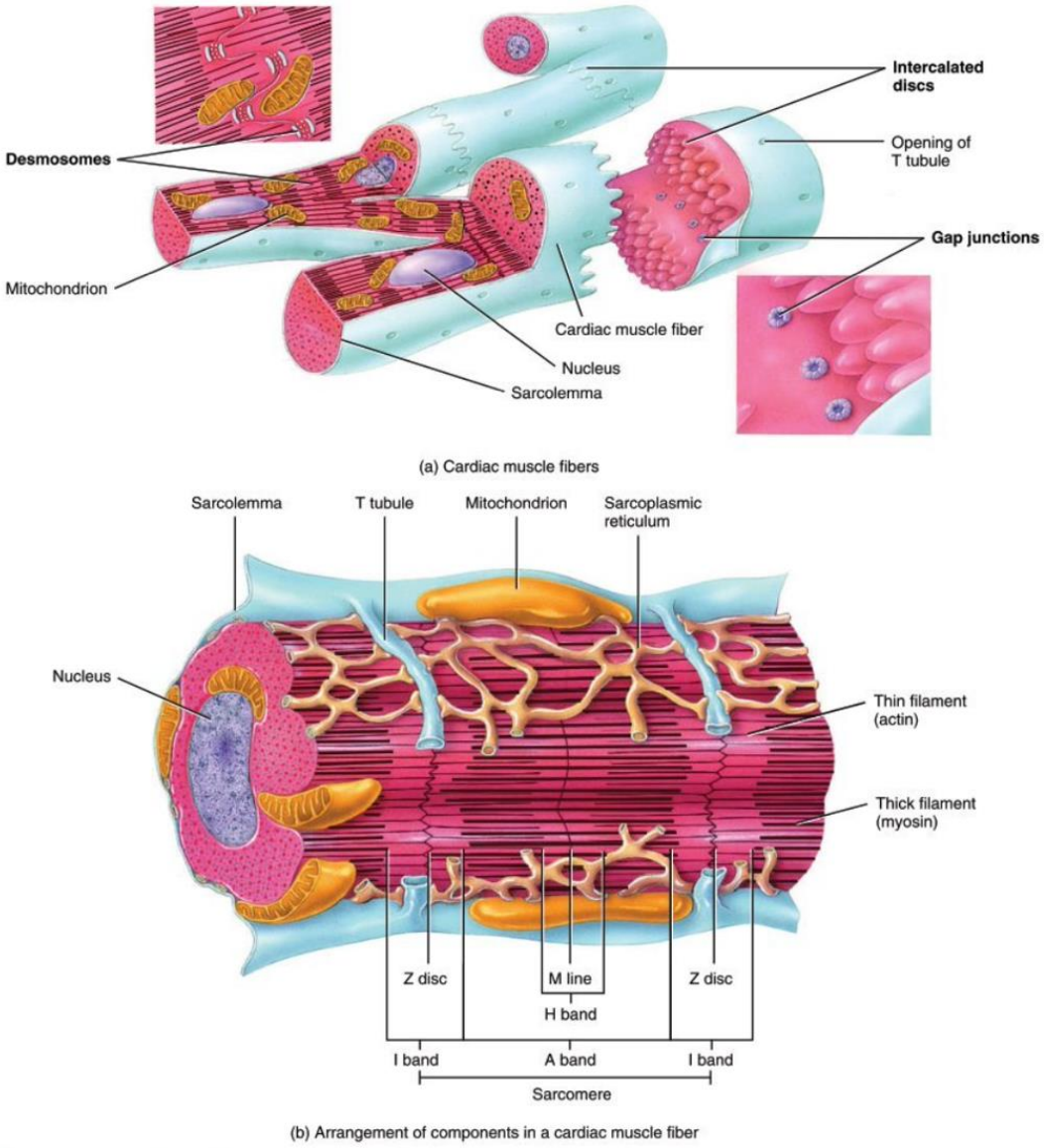

Figure 1. (Derrickson, 2021)

A typical cardiac muscle fiber is 50-100 μm in length and approximately 14 μm in diameter. These fibers typically contain a single nucleus, but occasionally, two nuclei can be present. The cardiac fibers are connected to nearby fibers through intercalated discs, which are part of the sarcolemma. Desmosomes, which hold muscle fibers together, and gap junctions that allow the propagation of action potentials between cells are both located in the intercalated discs. (Derrickson, 2021.)

2.3 Conduction system and action potential

The heart has a special impulse-conduction system to effectively contract and pump blood forward. The system consists of cardiac cells that are specialized to carry electrical impulses in the heart. (Arackal & Alsayouri, 2024.) The depolarization is made possible by various electrochemical gradients, which allow contraction of the cardiomyocyte. Uniform cardiomyocyte contraction provides a necessary force for every heartbeat that moves blood forward to the peripheric circulation. To maintain sufficient cardiac output, depolarizations must happen rhythmically, which ensures a normal heart contraction. (Tran et al., 2024.) The action potential (AP) originates from pacemaker cells and they also govern the rhythm. Pacemaker cells in the SA node usually govern the rhythm, but it can also be governed by cells in the AV node, a bundle of His, bundle branches, or Purkinje cells. The electrical impulse travels through T-tubules to every cardiomyocyte within the heart, creating contraction for a harmonious heart rhythm. (Arackal & Alsayouri, 2024.)

The cardiomyocyte AP is a process that contains five phases. All of the phases are important for the proper electrical functioning of the heart. Before the AP, the Phase 4 (resting phase) is present. This is maintained by K+ outflow. The process begins with Phase 0 when Na+ influx enters the myocyte through voltage-gated Na+ channels. This causes depolarization, and the membrane potential changes from -70 mV (resting phase) to +50 mV (depolarized phase). Phase 1 will follow after depolarization. This is where Na+ channels close and simultaneously K+ channels open, leading to K outflux. Next is phase 2, which includes Ca2+ influx through voltage-gated L-type Ca2+ channels. This causes the sarcoplasmic reticulum to release Ca2+, while K+ continues to leave the myocyte during this time. The rise of the intracellular calcium enables Ca2+ ions to bind to the Troponin C. This moves tropomyosin aside to allow actin to bind and the head of myosin to tint. This causes the proteins to slide, overlapping each other. After phase 2, Ca2+ channels will close, and K+ exits from the cell. The last phase of the AP is called Phase 3 (repolarization). This is facilitated by Ca2+-ATPase pumps or Na+/Ca2+ exchangers, which help restore Ca2+ to the sarcoplasmic reticulum. (X. Wei et al., 2024.)

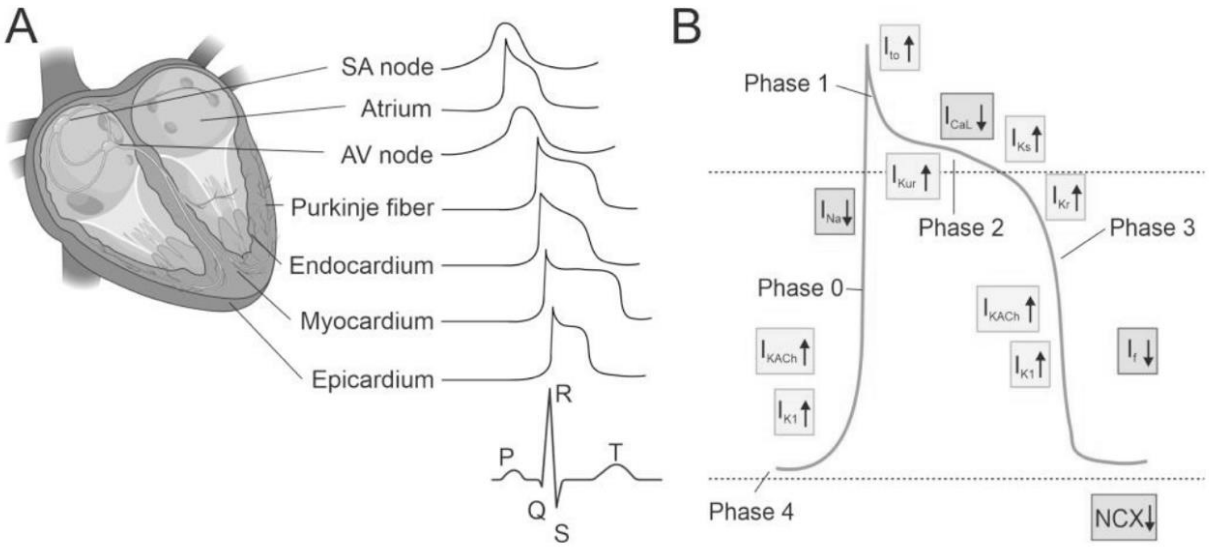

Figure 2. (Pekkanen-Mattila et al., 2019)

A. Cross-sectional view of the human heart with APs in different regions. The morphology and timing is different across the various areas of the heart and among different types of cardiomyocytes. These phases of AP also align with the surface electrocardiogram (ECG). B. AP have five phases where multiple ion currents have a certain role. Before AP begin, the myocyte cell membrane potential is in the resting phase (Phase 4). Phase 1 begins the AP, with the repolarization upstroke. Plateau phase (Phase 2) follows repolarization, and when cell membrane potential is decreasing back to the resting phase, it is called repolarization (Phase 3). (Pekkanen-Mattila et al., 2019.)

2.4 Coronary artery disease

Coronary artery disease (CAD) is one of the most common cardiovascular diseases. It can manifest in the form of stable and unstable angina, MI, or sudden cardiac death. (Álvarez-Álvarez et al., 2017.) CAD develops due to a process called atherosclerosis, which is characterized by inflammation and cholesterol accumulation in the subintimal space of the coronary artery (Malakar et al., 2019). Endothelial damage in the coronary arteries often occurs as a result of factors like hypertension, diabetes, or components found in tobacco. The CAD process begins when lipoprotein, and lipid droplets start to accumulate in the intima. As the disease progresses, the first findings are fatty streaks developed under the endothelial layer in the arterial walls. These fatty streaks are reversible, but if the disease progresses, vessel lumens narrow significantly, and clinical symptoms begin to manifest. Typical ischemic symptoms involve different manifestations of discomfort in the chest, upper limbs, jaw, or epigastric region. These occur usually during physical

activity, but symptoms are also possible while resting. The feeling of discomfort is typically not localized, positional, or influenced by the region's movement. Other symptoms related to ischemia may include manifestations such as dyspnea, syncope, diaphoresis/sweating, or exhaustion. (Thygesen et al., 2012.)

2.5 Stunning and ischemia

Insufficient coronary artery function will cause ischemia in the myocardium. This leads quickly to functional impairment and dysfunction. Unlike infarction, stunning is reversible and involves brief ischemic episodes that do not lead to irreversible myocardial necrosis or permanent damage. The dysfunction caused by stunning can persist from minutes to days. Stunning involves different levels of dysfunction in the myocardium depending on the ischemia duration. (Bolli & Marbán, 1999.) The dysfunction of myocardial stunning is thought to be influenced by three main factors. The first is the presence of free oxygen radicals, the second is calcium overload, and the third relates to decreased responsiveness of contractile filaments to calcium. CAD patients are a common group to suffer from myocardial stunning because of the narrower coronary arteries. (Braunwald & Kloner, 1982.)

2.6 Myocardial infarction

2.6.1 Definition and diagnosis

In the Third Universal Definition of Myocardial Infarction, the condition is described as the death of myocardial cells caused by prolonged ischemia due to insufficient blood flow (Figure 3.) in the coronary arteries (Thygesen et al., 2012). During ischemia, the myocytes do not die right away, the death occurs approximately in 20 minutes. In animal models, necrosis can be seen in a few-hour period (Thygesen et al., 2012), and it is eventually replaced by scar tissue (Arackal & Alsayouri, 2024). Patients suffering from STEMI or NSTEMI have an elevated risk of dying in the following month. The prognosis is better than in the 20th century, but the risk is still high. (Puymirat et al., 2017.)

The Third Universal Definition of Myocardial Infarction suggests that MI diagnosis is made when cardiac injury biomarkers (Troponin T or I) show an increase, in combination with at least one of these criteria: typical MI symptoms, findings in ECG, myocardial imaging evidence, or autopsy evidence. Elevated Troponin I and T are cardiac injury biomarkers for diagnosing MI. Diagnostic confidence increases if there is a noticeable rise or fall in troponin values. Repeated blood tests are often necessary to monitor trends in their levels. While elevated troponin levels are often related to MI, they can also be associated with other cardiac conditions. On an ECG, MI manifests

as a new ST-segment elevation at the J-point in two consecutive leads. The specific elevation criteria depend on the gender and age of the patient. Identification of an intracoronary thrombus, erosion of the endothelial surface, or plaque rupture to mechanically occlude the vessel can be visualized through angiography or other coronary visualization (e.g., OCT). To observe the heart during both acute and chronic phases of MI, various imaging techniques are commonly used. For instance, echocardiography (echo), radionuclide imaging, computed tomography (CT), and magnetic resonance imaging (MRI). (Thygesen et al., 2012.)

2.6.2 MI-types

The infarction can occur through various mechanisms. At the moment, there are five recognized MI-types. The first type, MI-type 1, is caused by the acute rupture, fissuring, ulceration erosion, or dissection of an atherosclerotic plaque. This will lead to an intraluminal thrombus of the coronary artery or arteries. The thrombus decreases the blood supply to the myocardium or causes distal platelet emboli, which results in cardiomyocyte death. The second mechanism, MI-type 2, is an imbalance in supplying and/or demanding oxygen to the myocardium. MI-type 3 three is described as a MI leading to death when the Troponin T or I values are unavailable. MI-type 4 and 5 are caused by percutaneous coronary intervention (PCI) or coronary artery bypass grafting or related to stent thrombosis. (Thygesen et al., 2012.)

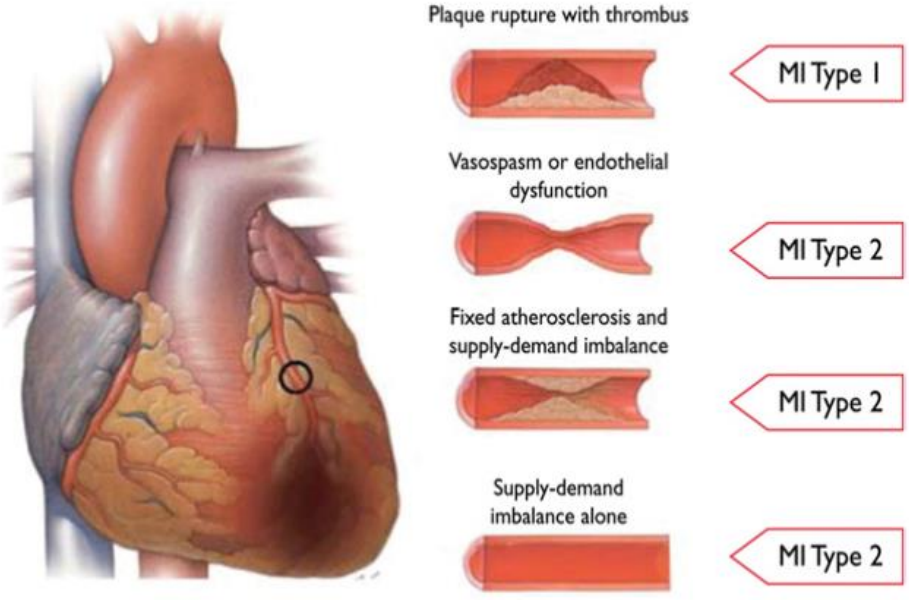

Figure 3. (Thygesen et al., 2012)

This figure illustrates the pathophysiological mechanisms underlying MI Type I and Type II. MI Type I is caused by a thrombotic mechanism. It represents spontaneous MI caused by acute

plaque rupture or erosion, leading to coronary thrombosis. In MI Type II, infarction happens due to ischemic imbalance. It can develop through various mechanisms, for instance: vasospasm, endothelial dysfunction, fixed atherosclerosis with a supply-demand mismatch, or supply-demand imbalance alone. (Thygesen et al., 2012.)

2.6.3 Heart failure and myocardial infarction

Heart failure (HF) is a syndrome in which the heart's ventricles cannot fill up appropriately anymore or loss of capacity to pass enough blood to the human body (St John Sutton et al., 2003). One of the most common causes of HF is MI (Mosterd & Hoes, 2007). After a MI, harmful remodeling occurs in the myocardium over time, which positively contributes to the risk of developing HF. For instance, structural (ventricular size and shape), functional, cellular, and molecular composition changes occur in the myocardium. The remodeling is thought to be due to immune pathway dysregulation, post-infarct decreased suppression of inflammation, and overactive fibrosis. (Prabhu & Frangogiannis, 2016.) For patients, remodeling causes a higher risk of hospitalization due to structural changes caused by MI. These can lead to increased end-systolic and end-diastolic volumes, which cause symptoms like pulmonary congestion and swelling of lower extremities and intestinal organs, e.g., the liver. (Sinnenberg & Givertz, 2020). Patients with HF have a high mortality rate after diagnosis. It has been observed that 5-year surveillance is 50%, and 10-year surveillance is 10% (Roger, 2013). In addition to the high mortality rate, it decreases life quality and lowers life expectancy (Jenča et al., 2021). For society, it causes a lot of expenses due to more frequent and longer hospitalization periods (Sinnenberg & Givertz, 2020).

2.7 Arrhythmias after ischemia or myocardial infarction

The proper spread of the depolarization wavefront in the heart is crucial for normal cardiac contraction (Good et al., 2021). Cardiac arrhythmias are disruptions in the heart's normal sinus rhythm. These can vary from minor variations in heart rate to multifactorial fibrillations (Han et al., 2021). Arrhythmias, such as ventricular tachycardia (VT) and ventricular fibrillation (VF), are serious complications of MI and cause a significant portion of sudden deaths linked to MI. These arrhythmias often occur alongside MI. 5.2 % of STEMI patients developed VT or VF before undergoing PCI, but some of them are linked to PCI procedure and reperfusion, i.e., the time following circulation to occur again. (Piccini et al., 2008.) VF or VT occurred in 8.9 % of cases following a primary PCI for STEMI. VT or VF events, which occur after 24 hours or later after PCI, are called late, and they affect 2.4 % of the patients. Although late arrhythmias are relatively rare after a PCI procedure, it is good to have in mind related to optimized hospitalization time. (Rymer et al., 2024.) Ventricular arrhythmias, occurring 2-3 days after MI, have a significantly high mortality

rate. Better outcomes have been linked with early arrhythmias, but mortality still occurs. (Frampton et al., 2023.) After MI, using of anti-arrhythmic drugs and implantable cardioverter defibrillators (ICD) are in an important role in managing ventricular arrhythmias (Bhar-Amato et al., 2017).

Arrhythmias are not only linked to structural remodeling, but ischemia also affects to arrhythmogenesis (Klabunde, 2017). During ischemia, reduced oxygen delivery to the myocardium leads to decreased ATP production in myocytes, negatively affecting their energy supply (Carmeliet, 1999). ATP-dependent ion pumps in the cell membrane fail to function due to the energy deficit. This alters the electrical properties of cardiomyocytes, significantly contributing to arrhythmogenesis and potentially triggering ventricular arrhythmias. (Klabunde, 2017.) Ischemia causes a decrease in conduction velocity (CV) (Good et al., 2021), and arrhythmias often arise after ischemia due to a decrease in electrical conduction (Hoeker et al., 2020) and the formation of conduction blocks that appear in the myocardium (King et al., 2013). If prolonged ischemia leads to infarction, an increased amount of collagen due to the infarct scar can lead to slower conduction in the heart, serving as an arrhythmogenic component (de Jong et al., 2011).

For patients who had a MI and survived, the remaining tissue heterogeneity makes them more prone to ventricular fatal arrhythmias (Schmidt et al., 2007). Arrhythmias are related with electrical and structural remodeling of the heart, which are often closely linked (Han et al., 2021). The size of the infarct, the diversity of the infarct scar tissue (Chowdhury et al., 2021), and the architectural and functional changes in the left ventricle are significant influencers to arrhythmia risk and make the heart more prone to arrhythmias later on (St John Sutton et al., 2003).

2.8 Border zone

2.8.1 Definition and characteristics

After a MI, the heart undergoes a dynamic healing and remodeling process (Prabhu & Frangogiannis, 2016), which occurs in both the ischemic region and the BZ (Wan Ab Naim et al., 2020). Scar tissue, which has a dense collagenous core, replaces necrotic cardiomyocytes. The area that surrounds this scar zone is the border zone (BZ). It is a thin layer of myocardium that survived the MI and is located between the healthy myocardium and the scar zone (Figure 4). (Mendonca Costa et al., 2018.) The myocardium can then be divided into three areas: the normally perfused and functioning healthy myocardium, the fully perfused but hypocontractile border zone, and the infarct area (scar zone). (Schelbert et al., 2010.)

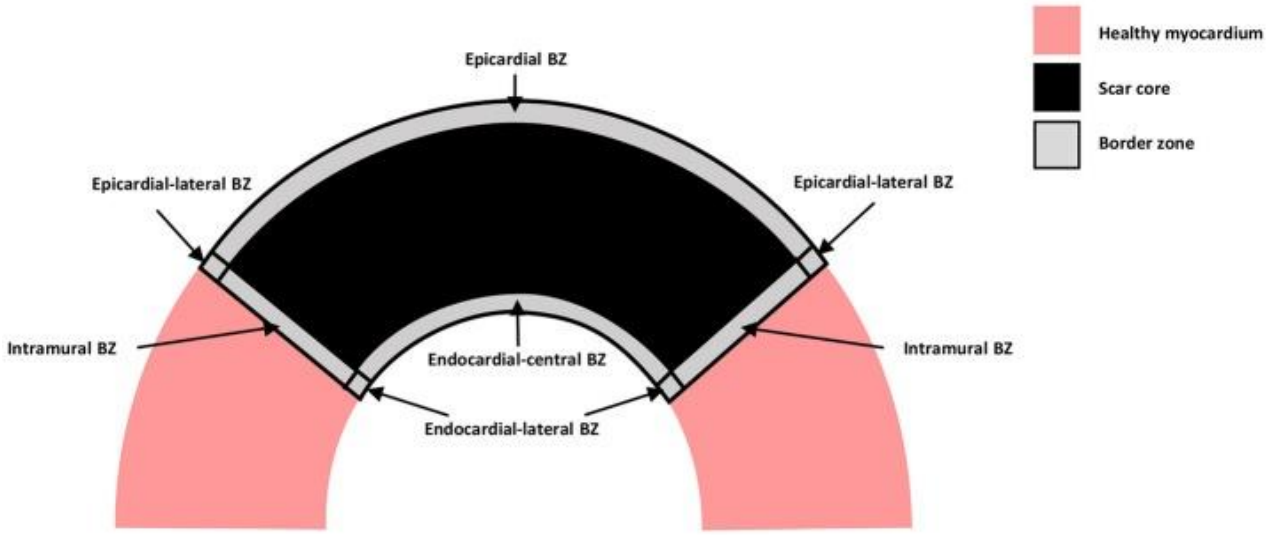

Figure 4. (Mendonca Costa et al., 2018)

Visual representation of transmural infarction. The BZ (grey) surrounds the scar area (black), and the healthy myocardium (pink) surrounds the BZ, which can be located epicardially, intramurally, or endocardially. (Mendonca Costa et al., 2018.)

The BZ represents as a transitional region between the normal functioning myocardium and the necrotic infarct zone. The transition from a healthy myocardium to the infarct area can be sharp, but there can be a mixture of healthy myocardium and patches or strands of fibrotic tissue in the BZ. (Schelbert et al., 2010.) The BZ tissue has reduced cellularity and disruption in the normal alignment of heart muscle cells. This is due to the area containing a mixture of living heart cells and fibrosis. The BZ also exhibits decreased tissue organization and an increase in disorganization of the fiber structure. (Kung et al., 2018.)

Significant cell size growth has been observed when comparing cells in the BZ to sham cells and non-infarcted epicardium in the 2-month follow-up time. (Dun et al., 2004.) On average, the width of BZ cells is significantly greater, while their length is not. In contrast, length of the myocytes in the remote region is greater. Cell size variability doesn't, although, show a correlation with action potential duration (APD) variability. (Amoni et al., 2023.) In an older study from Matthew Amoni (Amoni et al., 2021), only width showed a significant increase compared to cardiomyocytes.

2.8.2 Methods of investigation

The BZ is largely investigated, and large animal models have been seen as one of the best ways to recognize BZ regions after MI and link in vivo with ex vivo findings (Lindsey et al., 2018). The prevalent method for visualizing the BZ is through Cardiac Magnetic Resonance (CMR) imaging.

However, given the challenges and time-consuming nature of capturing the heart's electrical activity through CMR imaging, researchers have used utilized gradient on-a-chip (Rexius-Hall et al., 2022) and mathematical models derived from existing studies to visualize the BZ (Mendonca Costa et al., 2018).

2.8.3 Functional dysfunction

Despite being fully perfused, the BZ exhibits hypocontractility and undergoes expansion during the remodeling process. Initially, the BZ is a thin region next to the infarcted area. The BZ region is hypocontractile myocardium, although it is fully perfused. Over time, the BZ starts to expand by involving normally contracting and perfused myocardium. This leads to an expanding and larger hypocontractile zone that loses contractile function (Jackson et al., 2002). As remodeling progresses after MI, myocardial wall stress increases in the BZ area due to a reduction in endocardial curvature. (Jackson et al., 2003.) Weaker contractility in the BZ is partly due to the loss of sarcomere components, which are broken down by increased levels of matrix metallo proteinase-2 (MMP-2) (Spaulding et al., 2018).

The tissue changes after MI results in various functional complications in the BZ. The remodeling process causes ventricular dilatation and congestive HF due to the greater hypocontractility of the BZ (Jackson et al., 2003). Clinical signs of HF after MI in animal models appear between weeks 5 and 8. During this period, left ventricular diastolic pressure, end-systolic volume, ejection fraction, and stroke work all drop significantly while blood flow in the hypocontractile BZ remains similar to the remote areas. (Jackson et al., 2002.)

2.8.4 Altered ion dynamics

Remodeling of the cardiomyocytes' ionic currents in the BZ begins quickly, and after 5 days, changes can be seen (Mendonca Costa et al., 2018). In on-a-chip studies, tissues exposed to an oxygen gradient that mimics BZ exhibit slower calcium transient and delayed calcium release and reuptake (Rexius-Hall et al., 2022a). A decrease in Ca^{2+} current density in the BZ has been noticed in the two-month follow-up time in dogs' BZ. The BZ and remote areas of the healed heart infarct exhibit a slower calcium current recovery from inactivation, possibly due to generalized hypertrophic signals. (Dun et al., 2004.) There is a decrease in the L-type Ca^{2+} currents in the BZ (Weigand et al., 2017). The current has a crucial role in excitation-contraction coupling by allowing calcium to enter the cell when the cell membrane depolarizes (Nargeot et al., 1997).

Normal calcium dynamics influence both action potential and cardiomyocyte contraction. Calcium also has other vital functions, such as gene expression in the myocardium and other organs. Minor

changes in cardiac signaling due to disease, mutation, or long-term alteration of hemodynamic demand can lead to severe impacts on cardiomyocytes and the heart's function. (Fearnley et al., 2011.) During ischemia, oxygen levels decrease in the myocardium, which may lead to elevated intracellular calcium levels, increasing the risk of arrhythmias (Wan Ab Naim et al., 2020). This abnormal oxygen environment can disturb calcium cycling early in the infarction phase, inducing arrhythmias even without scar formation (Rexius-Hall et al., 2022).

As mentioned earlier, sodium and potassium play crucial roles in the depolarization and repolarization of cardiomyocytes (Kuo & Ehrlich, 2015). Also, calcium-dependent currents increase in the BZ during HF. There is an observed increase in Ca2+-activated K+ and Cl− currents, along with Ca2+ release-dependent delayed after-depolarizations. In the HF-border zone 5 months after MI, there is an increase in late Na+ current, a decrease in rapid delayed rectifier K+ current, and an inward rectifier K+ current. Also, it was noticed that the Na+/Ca2+ exchange current profile is altered. (Hegyi et al., 2018) Variations in individual ionic currents should be understood with caution when examining AP. These properties result from the complex interaction of multiple ionic currents rather than any single current alone. (Mendonca Costa et al., 2018.)

2.8.5 Electrical dysfunction and arrhythmia vulnerability

The electrical activity in the BZ after MI is disordered compared to healthy heart tissue, as demonstrated across various models, ranging from animal studies (Mendonca Costa et al., 2018) to on-chip experiments (Rexius-Hall et al., 2022) and mathematical simulations (Wan Ab Naim et al., 2020). Electrophysiological remodeling in the BZ is influenced by time, location (Figure 3.), and studied animals. Despite healing, ventricular arrhythmias in patients with MI are closely linked to the remodeling that occurs in the BZ. (Mendonca Costa et al., 2018.) Surrounding BZ contributes to arrhythmias (Baumeister & Quinn, 2016), and it is recognized to have structural and functional remodeling (Cabo & Boyden, 2006) and altered metabolism (Wong et al., 2012).

Decreased CV has been observed in isolated cells and tissues from failing hearts (Han et al., 2021). Similarly, a reduction in CV has been documented in the BZ, and it is partly due to the presence of fibrosis, which appears around 7 days after MI (Mendonca Costa et al., 2018). It is suggested that BZs' dysfunction is not primarily due to electrical activity but rather mechanical factors between ischemic and healthy myocardium (Ashikaga et al., 2005). However, both the mathematical model (Wan Ab Naim et al., 2020) and the on-a-chip study (Rexius-Hall et al., 2022) highlight the role of oxygen levels in influencing CVs in the BZ. In acute ischemia, CVs were decreased compared to normoxic conditions and were influenced by the direction of the action potential on-a-chip. Longitudinal speeds were unaffected by the direction relative to the oxygen

gradient, while transverse speeds were influenced by the gradient direction. Transitioning from hypoxic to normoxic conditions was not consistent, with slower conduction observed on the hypoxic side. (Rexius-Hall et al., 2022.) Lower oxygen concentration leads to decreased CVs also in a mathematical model, which divides the BZ into three zones based on electrical conduction: mild, moderate, and severely impaired. These areas of electrical conduction abnormalities expand over time. (Wan Ab Naim et al., 2020.) An optical mapping study on isolated hearts revealed that triggering VF at high activation rates is linked to a decrease in CV (Hernández-Romero et al., 2019). On the other hand, Mark L. Trew's research challenges the common notion of homogenous electrical changes in the BZ of chronic myocardial infarcts, with only focal delays in CV observed (Trew et al., 2019).

The APD in the BZ is not always normal, and it changes over time in the healing process, which has two phases: the healing phase (3 days to 5 weeks post-MI) and the healed phase (beyond 5 weeks post-MI). When BZ is in the healing phase, APD is generally shorter compared to healthy myocardium, but depending on the investigated animal, it can also be longer. The healed phase typically shows normal APD. Shortened APD can be seen after MI, with the most pronounced reduction occurring at 2 weeks. However, beyond this point, APD gradually increases and returns to normal levels after 8 weeks. (Mendonca Costa et al., 2018.) A longer-term study using pigs showed a reduction in APD in BZ 5 months after MI. Interestingly, at the same time, the remote, healthy zone of the heart exhibits APD longer than normal. (Hegyi et al., 2018.) Longer APD is a recognized outcome in ischemic myocardial cells (Klabunde, 2017). Other noted electrical impairments in the BZs' AP are decreased Plateau potentials, slightly depolarized resting membrane potentials (Hegyi et al., 2018), and a decrease in monophasic APs. (Weigand et al., 2017).

Electrical dysfunction makes BZ especially susceptible to re-entry arrhythmias. The BZ has longer and more variable activation-recovery intervals (ARIs), increased repolarization heterogeneity, the birth of premature ventricular complexes (PVCs), and association with reduced very low-frequency power. It has been noticed that the repolarization in the BZ area is more varied and longer when compared to the control sample. It has a broader distribution of regional ARIs compared to remote myocardial regions. In the research, the BZ was defined as a region with a CMR signal intensity of 20% to 70% of the maximum value, which is in the infarct core region. A study made with pigs (n = 8) showed that when arrhythmias are induced by VT induction, higher heterogeneity in ARIs and VT inducibility index (%) show a significant correlation. This variability is evident in cell population studies in vivo, where ARIs are generally longer and show more variability in the BZ. This is linked with an elevated risk of arrhythmias. The repolarization phase of action potential in the BZ is prolonged and more varied compared to remote regions of the heart after one month of MI. (Amoni

et al., 2023.) Repolarization heterogeneity is recognized is also supported by another animal model. In a living rat model with chronic ischemic HF, there is an increase in repolarization heterogeneity in the BZ compared to healthy myocardium (Weigand et al., 2017).

Another observed arrhythmia risk is that the BZ is linked with decreased very low-frequency power on heart rate variability analysis (Wong et al., 2012). In patients with MI with VT history vs. no VT history, the decreased very low-frequency power was identified as a strong independent indicator of VT susceptibility, and factors influencing low-frequency heart rate oscillations are linked to VT susceptibility (Huikuri et al., 1995).

2.8.6 Border zone on-a-chip oxygen gradient studies

There is a very limited amount of research on using on-a-chip devices where the BZ is modeled as an oxygen gradient. In a study by Megan L. Rexius-Hall, a BZ model was developed on-a-chip using neonatal rat ventricular myocytes. They created three different chips and exposed them to different oxygen conditions for four hours: normoxic (20 %), hypoxic (0 %), and oxygen gradient chip (20 % to 0 %). The gradient was obtained by utilizing two gas channels—one normoxic and one hypoxic. Compared to the normoxic side of the chip, the speed of both longitudinal and transverse CV decreases during acute ischemia in vitro compared to uniform normoxia. It was observed that, only transverse CV was influenced by the gradient's direction and was influenced by the location of the gradient. The transition from normoxic to hypoxic conditions was more consistent but occurred at a slower speed than under normoxic conditions. On the normoxic side, velocity was 0,1 cm / second faster vs. hypoxic. Transitioning from hypoxic to normoxic conditions was not consistent and occurred at a significantly slower speed compared to normoxic conditions. On the normoxic side, velocity was 2,2 cm / second faster vs. hypoxic. (Rexius-Hall et al., 2022.)

Additional observed characteristics were contractile dysfunction and elevation in the activity of signaling associated with inflammation. It was found that there were no notable differences in the gene expression of handling of calcium, propagation, contractility, or excitation-contraction coupling. The greater part of the dysfunctions observed in the oxygen gradient chip was not seen in the uniform hypoxia chip. This indicates that the observed tissue dysfunction in the gradient cannot be entirely connected to hypoxic oxygen levels. Tissues exposed to the oxygen gradient had slower calcium transients, delayed calcium release, and reuptake compared to hypoxic and normoxic chips. Heterogeneous expression of Connexin 43 (Cx43) was observed, with a significant increase in expression on the hypoxic side of the gradient compared to the hypoxic chip. Additionally, Cx43 protein expression was higher in the hypoxic channel of the gradient chip than in

the normoxic channel. (Rexius-Hall et al., 2022.) It's believed that the deceleration of CV is to result of factors like alterations in cell-to-cell coupling through Cx43 (Hoeker et al., 2020).

2.8.7 Can we treat the border zone?

BZ can lead to both long-lasting and acute heart problems, and some may be fatal for patients (Mendonca Costa et al., 2018). At the moment, there are no clinically available treatment options. It is believed that preemptive medical, catheter-based, or surgical strategies could potentially become viable treatments to prevent the expansion of the border zone and mitigate associated risks (Jackson et al., 2002). Here are some of the medical treatments that have shown reduced arrhythmia risk in the BZ using animal models.

SkM1-gene therapy has been found to reduce reentry arrhythmias in the epicardial BZ, with studies made with animals. After MI, the cardiac sodium channel (SCN5A) becomes mostly inactive, leading to decreased AP upstroke velocity (Vmax), slower conduction, and an increased risk of reentry arrhythmias. SkM1 is a rat skeletal muscle sodium channel. In an experiment, adenovirus carrying SkM1 fused with GFP (SkM1+GFP) was injected into the epicardial BZ. This made the BZ produce more SkM1 skeletal muscle sodium channels. A control group received only GFP. Electrograms from the epicardial BZ in sham-treated dogs were broad and fragmented (31.5 ± 2.3 ms), and from SkM1-treated dogs were narrower (22.6 ± 2.8 ms). Premature stimulation led to sustained VT or VF lasting more than 60 seconds in only 2 out of 12 SkM1-treated dogs compared to 6 out of 8 sham-treated dogs. These results suggest that overexpression of the SkM1 elevates V (max) in depolarization and decreases the incidence of stimulated, over 60 seconds, lasting VT and VF in dogs, who had MI. (Lau et al., 2009.)

Improving gap junction (GJ) connectivity function with rotigaptide leads to more uniform scar tissue formation in the BZ, reducing fibrosis irregularities without significantly altering infarct size. Rotigaptide is a drug that enhances GJ connectivity in myocytes. Given rotigaptide by osmotic minipump, rats' hearts treated 4 weeks post-MI exhibited a lower likelihood of arrhythmias during programmed electrical stimulation (rotigaptide inducibility score: 2.4 ± 0.8; control: 5.0 ± 0.6). These hearts also demonstrated reduced variability in scar tissue at the infarct BZ complexity dispersion score: rotigaptide: 1.1 ± 0.1; control: 1.4 ± 0.1) and improved CV in the BZ (rotigaptide: 43.1 ± 3.4 cm/s; control: 34.8 ± 2.0 cm/s). These results suggest that treatments targeting the morphology of the BZ can positively influence arrhythmia risk. (Ng et al., 2016.)

Overexpressing Sema3 in the BZ may reduce the vulnerability to ventricular arrhythmias by decreasing sympathetic hyper-reinnervation after MI. Sema3 is a chemorepellent that inversely relates to sympathetic innervation. The research was done with adult male Sprague-Dawley rats (n

= 60). The rats were divided into different treatment groups: the phosphate-buffered saline (PBS) group, the mock lentivirus (MLS) group, and the lentivirus group that causes overexpression of Sema3a (SLV). All rats underwent a MI procedure involving the LAD, and six hours later, each rat received an injection into the BZ with the treatment. Programmed electrical stimulation was done to all groups. A significantly shorter QTc interval was observed in the SLV group compared to the MLV and PBS groups. VT was induced, and the SLV group showed a significantly lower incidence of VT and lower arrhythmia scores compared to the other groups. QTc interval, VT inducibility, and arrhythmia scores were close to each other in the SLV and control group, and The PBS and MLV groups had significantly higher arrhythmia scores. (R.-H. Chen et al., 2013.)

Doxycycline infusion following MI was investigated for its effects on MMP-2 levels. Sustained improvements were achieved in the BZ by normalizing MMP-2 levels. Six weeks after MI, better contractility was observed ex-vivo and increased end-systole wall thickness. The mechanism is not fully understood, but these improvements were associated with reduced intracellular MMP-2 activity. The proposed mechanisms are that doxycycline non-selectively inhibits MMPs by chelating the structural Zn2+ essential for their catalytic activity, and doxycycline can suppress MMP transcription. In addition to these effects, doxycycline functions as a free radical scavenger and exhibits anti-apoptotic and immune-modulatory properties. (Spaulding et al., 2018.)

2.9 hiPSCs

2.9.1 Definition and characteristics

One way to model human cardiomyocytes is to use human induced pluripotent stem cells (hiPSCs). These cells can be differentiated into any cell types, such as hiPSC-cardiomyocytes (hiPSC-CMs). There are several benefits when utilizing hiPSC-CMs in a laboratory environment used in an OxyGenie mini-incubator combined with a microelectrode array (MEA). This enables real-time monitoring and control over oxygen levels. This trait allows to use hiPSC-CMs to model different cardiovascular diseases and explore potential therapeutics. A disadvantage is that their metabolism resembles more fetal state cardiomyocytes because hiPSC-CMs rely their metabolism on glucose, making it better to handle hypoxic conditions, whereas adult cardiomyocytes rely on fatty acid oxidation, which makes them more susceptible to oxidative stress compared to adult cardiomyocytes. (Häkli et al., 2021.)

2.9.2 hiPSCs in hypoxic conditions

However, using hiPSC-CMs are proper way to model ischemic-reperfusion injury. It has behaved similarly in ischemia compared to reported results with former knowledge. For instance, observed

issues in hypoxia include a decrease in beating frequency, prolonged depolarization time, reduced overall field potential duration (FPD), and decrease in signal propagation speed (longer APD). In hypoxia, hiPSC-CMs show decreased beating frequency and field potential amplitude, initially dropping (lowest at 7-15 h). Yet, from 15–24 hours, beating frequency gradually increases, signifying adaptation to low oxygen. Upon reoxygenation, beating frequency surpasses baseline before returning. Field potential duration decreases in hypoxia, causing longer depolarization times, but reverts to baseline after reoxygenation. CV across hiPSC-CM sheets slows during hypoxia, extending APD. (Häkli et al., 2021.)

Additional phenomena noted in the hypoxic conditions were cell death, disruption of the sarcomere structure, decrease in contractility, calcium overload, and arrhythmias (T. Chen & Vunjak-Novakovic, 2019). The alterations noticed in the electrophysiological characteristics of hiPSC-CMs resembled the changes typically seen in adult cardiomyocytes during heart ischemia and reperfusion. (Häkli et al., 2022.)

3 Methods

3.1 The aim of the study

Our objective is to observe changes in nuclei size, sarcomere, and myocyte structure of the hiPSC-CMs within an oxygen gradient chip. Simulating the myocardium's BZ after a MI to understand how varying oxygen levels influence the integrity of myocardial cells. For this purpose, we utilized a specialized oxygen gradient chip (developed at CoEBoC Tampere University), with oxygen levels ranging from 0 % to 19 %. The distance between two gas pipes is 2,5 mm. The hypoxic end of the gradient mimics the area of the heart during MI that has lost normal blood flow, while the normoxic end represents the healthy, well-perfused myocardium. Gas with 19 % oxygen saturation is typically used in incubators, and it creates good conditions for the hiPSC-CMs. The BZ lies between these two regions. We aim to investigate whether this oxygen gradient impacts myocyte structure by comparing conditions in the gradient with normoxic (normal oxygen levels) and hypoxic (low oxygen levels) environments.

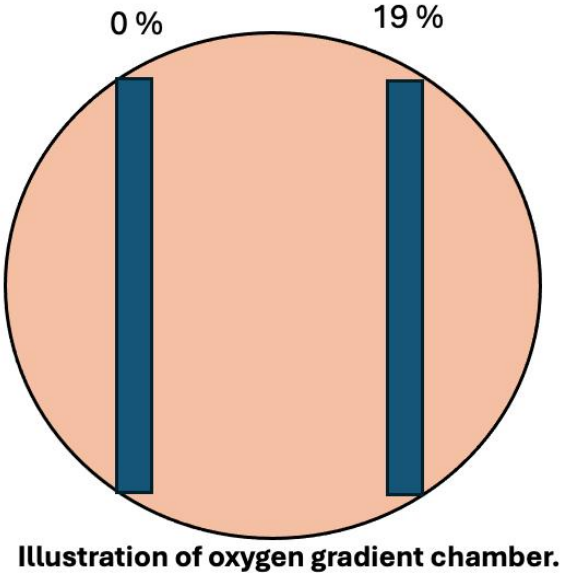

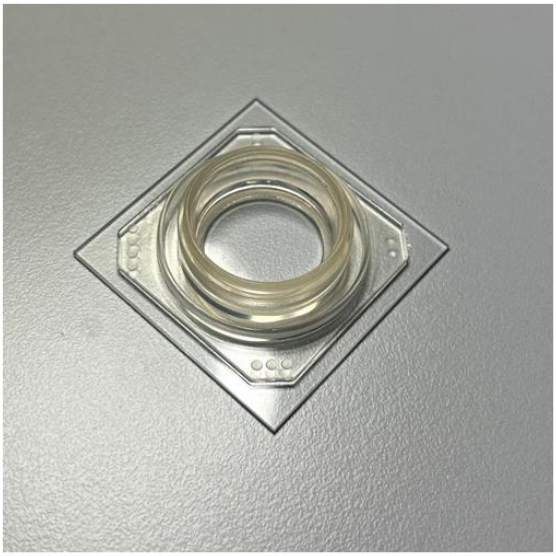

Figure 5. On the left is an illustration of the oxygen gradient chamber from above. The blue columns represent gas tubes that provide a hypoxic environment for the left side of the chamber and normoxia for the right side of the chamber. Between the two blue columns is the oxygen gradient, which mimics the border zone of the heart. The hiPSC-CMs are in the orange circle area of the illustration. On the right is a picture of the chamber without the gas tubes and cells.

3.2 Ethical considerations

In this study, we are using hiPSC lines reprogrammed by the Heart Group at Tampere University. The Pirkanmaa Hospital District's ethics committee granted the Heart Group permission to derive hiPSC lines from donor skin biopsies (Aalto-Setälä R08070). The Heart Group has approval for differentiating these hiPSCs into cardiac cells (Aalto-Setälä R12123). All donors provided informed consent in writing.

3.3 The cell preparation process and differentiation

The hiPSC-CMs used in the experiment were differentiated from cell line 11311. The iPSC-CMs were differentiated by using the hEB-protocol (Prajapati et al., 2021). The only difference is that we are using KSR at day 0 instead of using the mTeSR1 medium that was used in the article.

3.4 Dissociation and Magnetic-activated cell sorting

After differentiation, we used the dissociation protocol (Mummery et al., 2003) to dissociate the cells. Beating embryoid bodies (EBs, three-dimensional aggregates formed by pluripotent stem cells) were transferred into the same well. Media was removed and cardiomyocyte dissociation protocol was started with Low-Ca buffer, intubated mistakenly at 37 degrees instead of room temperature. The enzyme medium was incubated at room temperature for 45 minutes. KB medium was incubated at room temperature for 1 hour. Then 20 % EB medium was added, and EBs were broken down. The next step involved the Magnetic-activated cell sorting (MACS) protocol, which separates hiPSC-CMs from other cell types that may interfere with the study, i.e., making the cell population purer. The whole process is done with MACS- MultiTissue Dissociation Kit 3 (Miltenyi Biotec, Bergisch Gladbach, German) using the instructions with it. After MACS-protocol, the sorted cells were plated on the chip chambers. The cells were grown and prepared for gradient experiment by changing the EB medium every other day.

3.5 Exposure to the oxygen gradient and Double Fluorescence protocol

Before the exposure of the hypoxia gradient, the cells were checked with a microscope (Nikon Eclipse TS100-phase contrast microscope). Important was to notice that the cells are pulsating. Then, the cells were exposed to three different oxygen conditions for 24 hours. One is normal oxygen at 19 %, the second is 0 % oxygen, and the third is the oxygen gradient of 0 % - 19 %.

Immunocytochemistry was performed after gradient exposure using the Double Fluorescence protocol (Ojala et al., 2012), which is designed to ensure accurate visualization and analysis of

these cellular components, for instance, nuclei sizes, sarcomere structure, and the overall morphology of hiPSC-derived cardiomyocyte. First, the cells were fixed and then dyed by the Double-Fluorescence protocol. Initially, the cells undergo a washing step with phosphate-buffered saline (PBS, Lonza). Then, cells were fixed for 20 minutes with 4 % paraformaldehyde (PFA, Sigma-Aldrich). After fixation, the cells were permeabilized and blocked with 10 % normal donkey serum (NDS, Sigma-Aldrich), Triton X-100 (Sigma-Aldrich), and 1 % bovine serum albumin (BSA, Sigma-Aldrich) in PBS 45 minutes at room temperature, and stained with primary antibodies: mouse anticardiac TroponinT (1:500, Abcam) and MYBPC (1:400, Santa Cruz Biotechnology) diluted in 1 % NDS, 0,1 % Triton X-100, and 1 % BSA in PBS overnight in 4+ C. The next day, three 5-7 min washes were done with 1 % BSA in PBS. Next, secondary antibodies were diluted in 1 % BSA in PBS for one hour at room temperature. Antibodies are the following: Alexa Fluor 488 anti-mouse (1:800, Thermo Fisher Scientific) and 568 anti-rabbit (1:800, Thermo Fisher Scientific). After the secondary antibodies, the cells are dried and mounted with Vectashield (Vector Laboratories Inc.), and coverslips are applied. Vectashield contains 40,6-diamidino-2-phenylindole (DAPI) for nuclear staining. Finally, the samples are stored at 4°C and protected from light before the imaging.

3.6 Examining cells and statistics

Four samples were examined and imaged under a Leica microscope with 5x, 10 and 20x objectives after Double-Fluorescence protocol. TroponinT staining was used to identify cardiomyocytes from other cell types. Troponin is a protein involved in myocyte contraction. DAPI on the other hand, stains the nuclei of all cells. By staining both sarcomeres and nuclei, we were able to clearly identify which nuclei belonged to myocytes and differentiate them from other cells.

The primary focus was on the sarcomere structures within the cells and nuclei sizes in myocytes. Nuclei sizes were manually analyzed with the Fiji measurement tool. Nuclear length was defined as the longest axis, while the width was defined as the shortest axis. In total, 12 nuclei were measured in each group. Statistical analyses were conducted in SPSS, with the oxygen gradient group compared to the other groups using the Mann-Whitney test.

4 Results

In this study, hiPSC-CMs were exposed to oxygen gradient (0 % – 19 %), normoxia (19 %), or hypoxia (0 %) for 24 hours. The sarcomere structure and nuclei sizes were investigated with immunocytochemical staining of MYBPC3 and TroponinT. The cardiomyocytes were identified from other cell types based on positive staining.

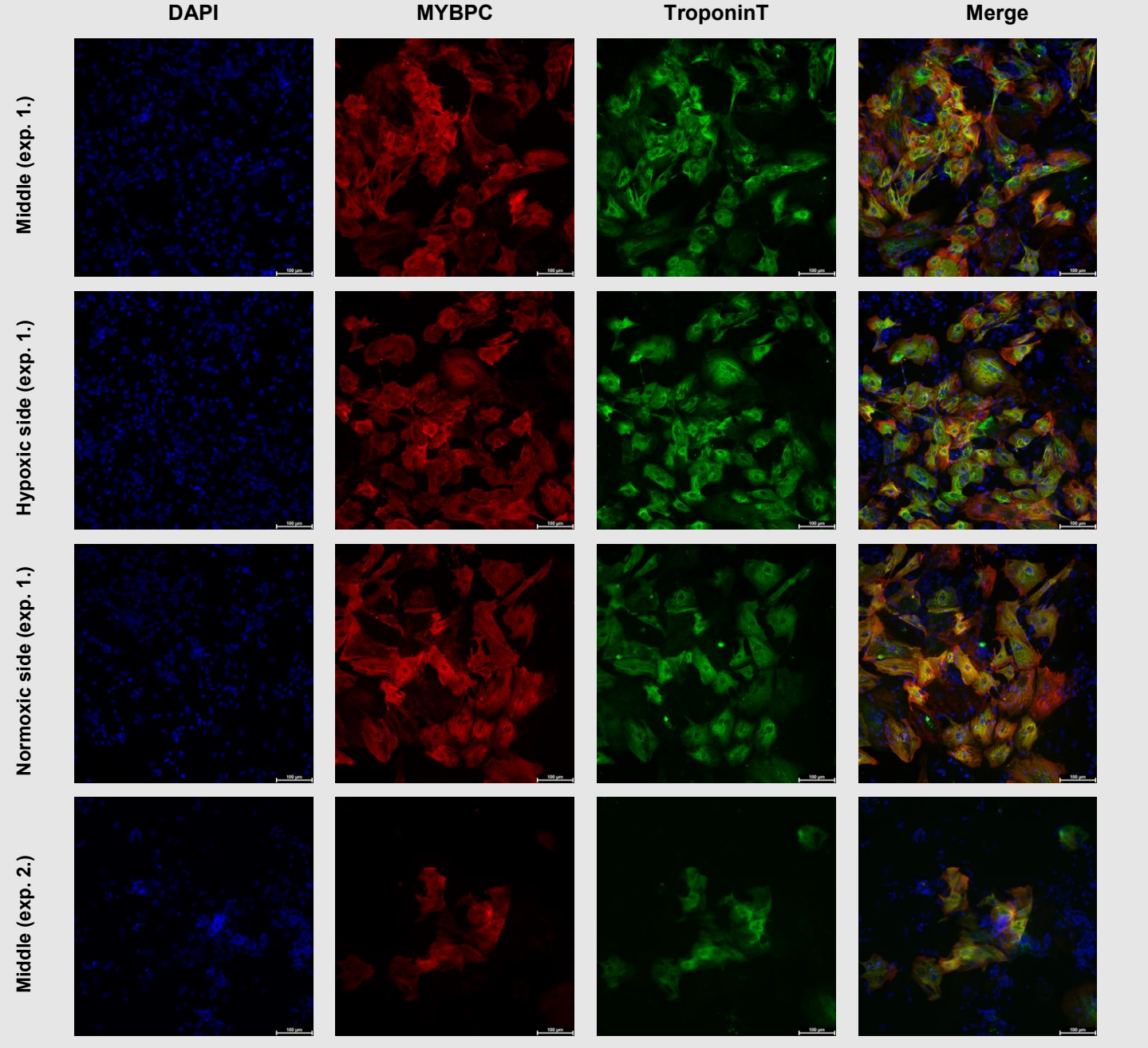

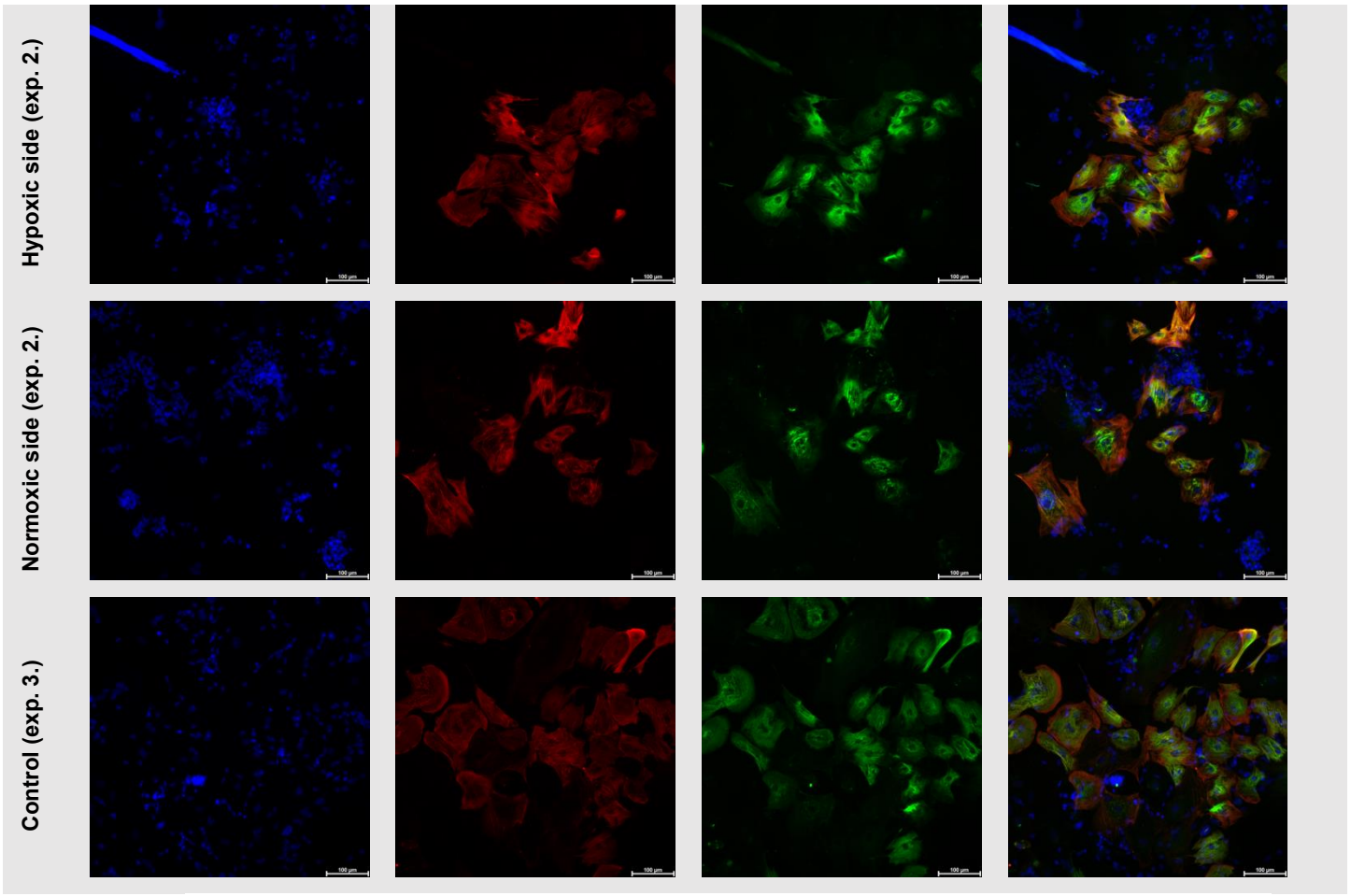

Figure 6. Experiments. 1. and 2. are from oxygen gradient, and experiment 3. is from uniform normoxia. Oxygen levels are in the middle of the oxygen gradient (0 - 19 %), the hypoxic side of the gradient (0 %), and the normoxic side of the gradient (19 %). The control sample is from uniform normoxia. The colors are blue (DAPI), red (MYBPC), and green (TroponinT). Pictures are taken with 20x objective, and scale bars are 200 µm. All cells did survive in different oxygen conditions, and no signs of breakdown of cell structure was observed. The sarcomere structures of the cells did not exhibit changes.

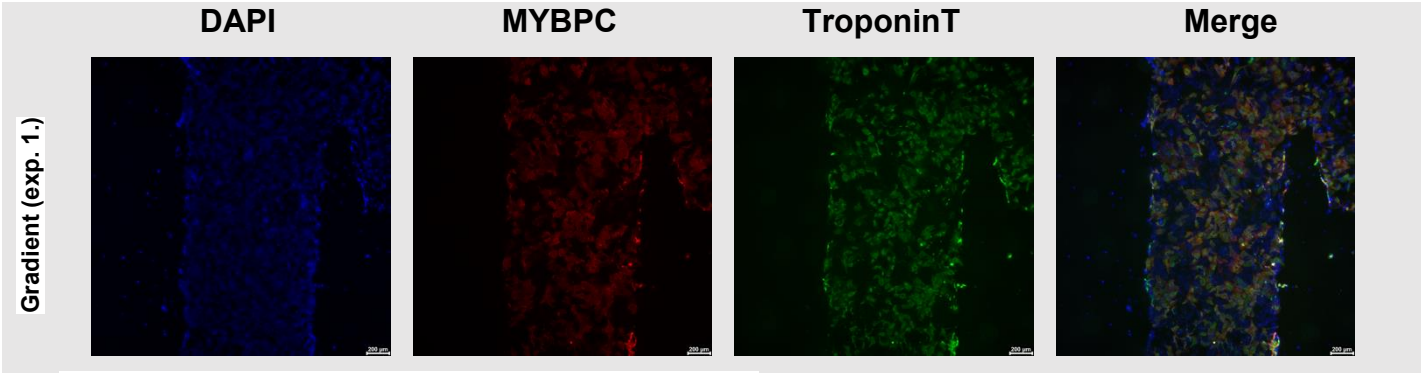

Figure 7. Overview of the gradient from experiment 1. Fluorescent pictures of hiPSC-CMs after 24 hours of exposure to different oxygen levels. Imaged with 5x objective. Dark spots can be seen on both sides of the gradient; these are the spots of the gas tubes, and the cells are badly stained and damaged.

4.1 Overview of the hiPSC-CMs and sarcomere structure

After the pictures were taken of the myocytes with a Leica microscope, we analyzed the overview of the myocytes. In the overview image (Figure 7), DAPI, MYBPC, and Troponin T staining are clearly visible across different sections of the gradient, indicating preserved cellular structure. Notably, only the cells located directly beneath the gas tubes were not measured.

In a closer view (Figures 6. and 8.), there were no observed differences between the hypoxic and normoxic sides within the oxygen gradient chamber. Tissue organization remained intact across all samples, i.e. we found no signs of destruction of cell structure or morphological changes. In hypoxic or other conditions, we observed no cell swelling, membrane rupture, or fragmented cell borders. Interestingly, even on the hypoxic side of the gradient, the sarcomeres displayed an organized and striated pattern. Nuclei visualize easily with DAPI, and there is no fading or loss of nuclear staining.

The cellular architecture of the cardiomyocytes (MYBPC and TroponinT) appears well-organized and structurally intact across all samples. The sarcomeres exhibit a highly organized and striated pattern, with clear striations visible. This organization was consistent across both oxygen gradient and hypoxic conditions, showing no significant differences. This confirms the preservation of an optimal and functional cellular arrangement practically throughout the gradient.

Control sample **Normoxia**

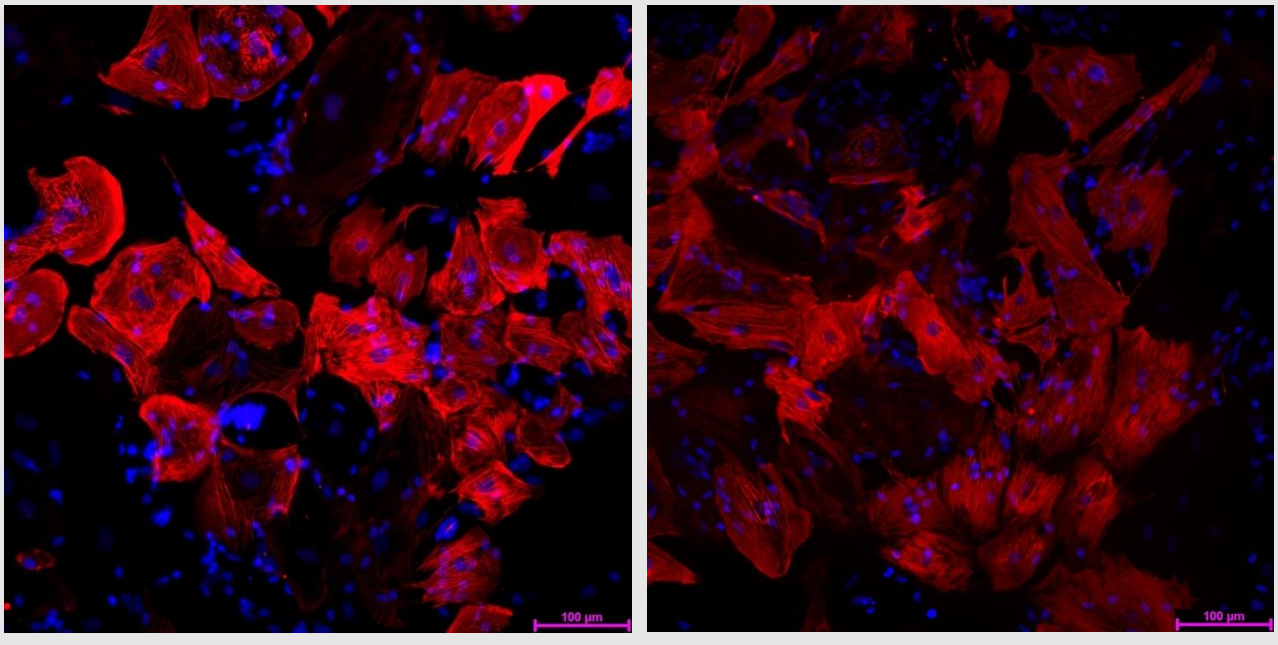

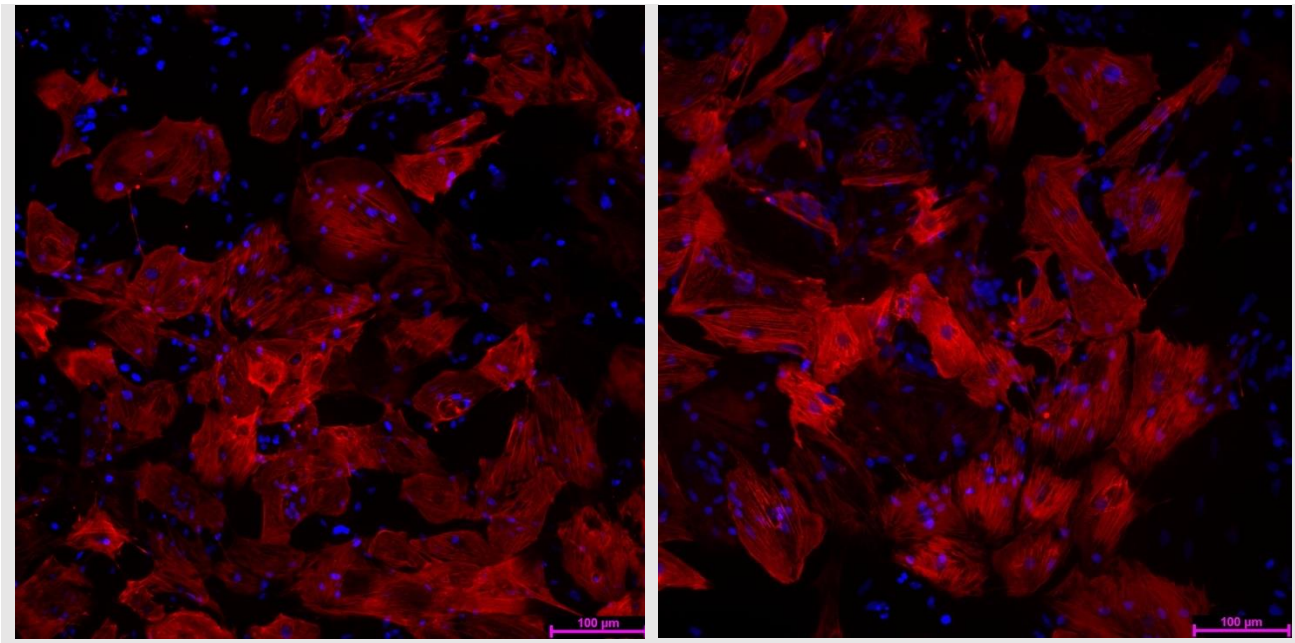

Figure 8. Fluorescent pictures (TroponinT + DAPI) of the nuclei that were measured form experiment 1. Blue colors (DAPI) represent the nuclei in the sample and red color (TroponinT) shows the cell myocyte cell structure. The scale bar is 100 µm. The upper left corner is the control sample. The upper right corner is from normoxia. The left sample downer sample is from hypoxia. The right downer sample is from the oxygen gradient. Cells measured from these pictures revealed that in hypoxic conditions, the cells' nuclei were smaller compared to normoxia and oxygen gradient (Figure 9.).

4.2 Nuclei sizes

The second aspect that we examined was the sizes of the nuclei in different conditions. The nuclei were investigated through a Leica microscope with a 20x objective. By using the the Fiji measuring tool, the results are the following. In an oxygen gradient, the nucleus has an average length of approximately 12.49 µm and a width of 6.45 µm. Under hypoxic conditions, the nucleus size decreases, with an average length of 10.57 micrometers and a width of 6.43 µm. In normoxic conditions, the nucleus is larger, measuring an average of 13.51 µm in length and 7.16 µm in width. The control sample has an average nucleus length of 12.33 µm and a width of 6.70 µm. Overall, cell nuclei in hypoxia are smaller compared to those in other conditions in measured cells. (Figure 8.)

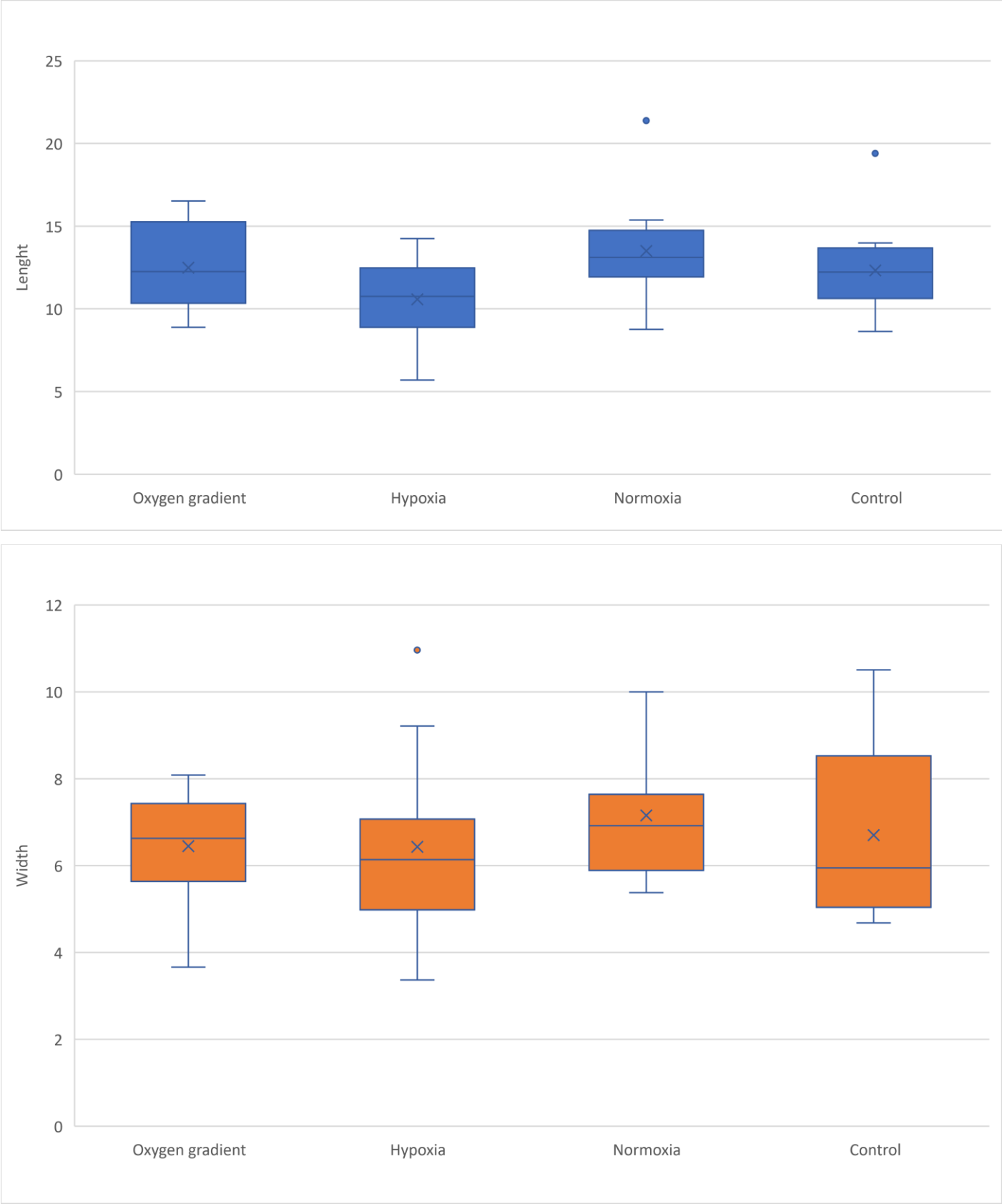

Figure 9. The chart shows the sizes of cell nuclei in four different conditions: in oxygen gradient, hypoxic side of the gradient, normoxic side of the gradient, and in the control sample. Nuclei sizes are measured from experiment 1. The cells exhibited the widest range of nuclei lengths

under the normoxic side of the gradient. The nuclei lengths varied from 8.758 µm to 21.389 µm, while widths ranged from 5.379 µm to 9.499 µm. In the oxygen gradient, nuclei lengths ranged from 8.883 µm to 16.528 µm, and widths varied from 5.600 µm to 8.084 µm. Under the hypoxic side of the gradient, nuclei lengths ranged from 5.696 µm to 14.256 µm, with widths varied between 4.798 µm and 10.963 µm. On the hypoxic side, the cells exhibited the widest range of nuclei widths. In the control sample, nuclei lengths varied from 8.637 µm to 19.397 µm, and widths ranged from 4.678 µm to 10.503 µm.

Length			
	Median values	**Percentiles 25**	**Percentiles 75**
Oxygen gradient (1)	12.251	10.343	15.257
Hypoxia (2)	10.762	8.878	12.475
Normoxia (3)	13.118	11.939	14.748
Control (4)	12.221	10.637	13.678
	Comparing lengths (Mann-Whitney test)		
Comparison	1 & 2	1 & 3	1 & 4
p-values	p = 0.101	p = 0.514	p = 0.887

Width			
	Median values	**Percentiles 25**	**Percentiles 75**
Oxygen gradient (1)	6.625	5.635	7.428
Hypoxia (2)	6.138	4.978	7.069
Normoxia (3)	6.916	5.890	7.639
Control (4)	5.948	5.039	8.526
	Comparing widths (Mann-Whitney test)		
Comparison	1 & 2	1 & 3	1 & 4
p-values	p = 0.478	p = 0.319	p = 0.932

Figure 10. There was no significant difference in nuclei sizes in length or width when comparing the oxygen gradient group in the hypoxia, normoxia, or control samples. The Mann-Whitney test was used to obtain the results. The median value better describes the whole, as there were individual large nuclei in some of the samples.

5 Discussion

This study aimed to determine whether the oxygen gradient on-a-chip affects hiPSC-CMs' sarcomere structure or the nuclei sizes. We hypothesized that in an oxygen gradient, hiPSC-CMs' nuclei would be smaller compared to the control sample. The second hypothesis is that disruption of the sarcomere structure or destruction of cell structure would be present.

Before our experiments began, we confirmed the presence of an oxygen gradient on-a-chip in two separate tests without the hiPSC-CMs. Additionally, the well that contained the chip has been proved as an effective method for modeling the ischemia with hiPSC-CMs (Häkli et al., 2022). This reliability supported us to use the same well, as it had been established as a suitable method for gradient studies. In this research, we did not verify the presence of an oxygen gradient, i.e., ensure the oxygen content at different points of the chip before or during the experiments. After the oxygen exposure, nuclei sizes were measured manually. We measured 12 nuclei sizes from each group to reduce human error and obtain a more accurate average.

After the experiments and measurements, our results did not support the hypotheses. The purpose was to create border zone-like oxygen conditions for the hiPSC-CM. We hypothesized similar changes could be present on-a-chip compared to uniform hypoxia because the exposure time was 21 hours longer. hiPSC-CMs undergo significant cellular changes (smaller nuclei sizes, distribution of cell structure, and cell death) after three hours of exposure to uniform hypoxic conditions within the same well used for our gradient studies (Häkli et al., 2022). Those changes we were not able to observe in any of our experiments. We observed no cell death, fading, or loss of nuclear staining. No significant difference (Figure 10.) in nuclei sizes in length or width when we compared the oxygen gradient group in the hypoxia, normoxia, or control sample (Figure 9.). Nuclei sizes were smaller in hypoxia compared to other groups, but no significant differences were noticed compared to the oxygen gradient (Figure 9.). Sarcomere structure was the second studied aspect, which was evaluated visually from the pictures (Figure 6. and Figure 7.) The structure was highly organized and had a striated pattern, with clear striations visible in all of the samples.

Previous research related to hypoxia (Häkli et al., 2022) and border zone a-a-chip (Rexius-Hall et al., 2022b.) studies indicated that cell changes would be present. The results that we observed, did not fulfill our hypotheses. It is possible that the well we used, did not work as we wanted with the hiPSC-CMs. Earlier tests confirmed that the gradient on-a-chip functioned correctly in the absence of cells. This indicated that the chip itself was reliable under controlled conditions. A few factors

might explain why we did not observe similar cell structural changes that we hypothesized, and which have been documented in hypoxic conditions before with hiPSC-CMs. First, the dimensions of the oxygen gradient chamber were not sufficient, and the distance between the two gas channels might have been too narrow in order to form an oxygen gradient. This environment may have allowed well-oxygenated cells to compensate for the hypoxic ones, which helped to maintain overall cellular function and structure, and it may have reduced the hypoxic environment's impact. This compensatory effect was noticeable when examining nucleus size, sarcomere structure, and overall cell architecture. All of them remained essentially unchanged despite variations in oxygen levels. The cells, which were located near the hypoxia gas tube likely received a significant amount of oxygen from neighboring cells, which reduced the overall effect of the hypoxic environment. Second factor that has been taught to be behind the results is gas leakage. Leakage might have come from the outside of the chamber, and have resulted in less severe hypoxia than intended, leading to more oxygenated areas in the well.

To overcome these challenges in future on-a-chip studies, it is important to develop a broader oxygen chamber that could reduce compensatory effects in myocytes. A second aspect is to ensure the oxygen content at different points of the chip before the experiments. The development of the chamber is essential because the gradient on-a-chip holds significant potential for studying the border zone in cardiac research. While cell structures are stained using animal-derived dyes, this method is more ethical than inducing myocardial infarctions in live animals for research purposes. The imaging process benefits from the simplicity of using a Leica microscope. Using the microscope allows for clearer observation to concentrate on a small number of cells. During acute ischemia, we are able to watch how they behave, which is more straightforward than cardiac magnetic resonance (CMR) imaging with a living animal model. Despite these strengths, CMR imaging and living animal models also have their own place when observing a larger-scale heart function. Aspects that could be investigated in the future with oxygen gradient on-a-chip are electrophysiological differences, arrhythmias, gene expression, and ion currents. These are important for understanding the complexities of the border zone and should be addressed in future research. Measuring these variables will improve our ability to pinpoint the specific vulnerabilities of the border zone and its susceptibility to dysfunction. If we cannot see changes in a short follow-up time, a longer exposure time to the gradient, or extending the follow-up time over several weeks or even months to see the impact of the gradient.

6 Conclusion

The purpose of the study was to find out whether the oxygen gradient impacts the sarcomere structure or the nuclei sizes on-a-chip. We hypothesized that in an oxygen gradient, hiPSC-CMs' nuclei would be smaller compared to the control sample, and harmful changes occur in the sarcomere structure. We did not observe any changes that we hypothesized. There was no significant difference in hiPSC-CMs' nuclei sizes when comparing oxygen gradient to other samples. The cells in the oxygen gradient maintained their cell structure. Oxygen gradient on-a-chip research has a lot of potential due to ethical reasons and the possibility of observing the cells very closely with a microscope. In the future, the goal is to improve the functionality of the oxygen gradient chamber in research operations by making it wider and more reliable so that no gas leakage is possible.

References

Álvarez-Álvarez, M. M., Zanetti, D., Carreras-Torres, R., Moral, P., & Athanasiadis, G. (2017). A survey of sub-Saharan gene flow into the Mediterranean at risk loci for coronary artery disease. *European Journal of Human Genetics : EJHG*, *25*(4), 472–476. https://doi.org/10.1038/ejhg.2016.200

Amoni, M., Vermoortele, D., Ekhteraei-Tousi, S., Doñate Puertas, R., Gilbert, G., Youness, M., Thienpont, B., Willems, R., Roderick, H. L., Claus, P., & Sipido, K. R. (2023). Heterogeneity of Repolarization and Cell-Cell Variability of Cardiomyocyte Remodeling Within the Myocardial Infarction Border Zone Contribute to Arrhythmia Susceptibility. *Circulation. Arrhythmia and Electrophysiology*, *16*(5), e011677. https://doi.org/10.1161/CIRCEP.122.011677

Arackal, A., & Alsayouri, K. (2024). *Histology, Heart*.

Ashikaga, H., Mickelsen, S. R., Ennis, D. B., Rodriguez, I., Kellman, P., Wen, H., & McVeigh, E. R. (2005). Electromechanical analysis of infarct border zone in chronic myocardial infarction. *American Journal of Physiology. Heart and Circulatory Physiology*, *289*(3), H1099-105. https://doi.org/10.1152/ajpheart.00423.2005

Baumeister, P., & Quinn, T. A. (2016). Altered Calcium Handling and Ventricular Arrhythmias in Acute Ischemia. *Clinical Medicine Insights. Cardiology*, *10*(Suppl 1), 61–69. https://doi.org/10.4137/CMC.S39706

Bhar-Amato, J., Davies, W., & Agarwal, S. (2017). Ventricular Arrhythmia after Acute Myocardial Infarction: "The Perfect Storm". *Arrhythmia & Electrophysiology Review*, *6*(3), 134–139. https://doi.org/10.15420/aer.2017.24.1

Bolli, R., & Marbán, E. (1999). Molecular and cellular mechanisms of myocardial stunning. *Physiological Reviews*, *79*(2), 609–634. https://doi.org/10.1152/physrev.1999.79.2.609

Braunwald, E., & Kloner, R. A. (1982). The stunned myocardium: prolonged, postischemic ventricular dysfunction. *Circulation*, *66*(6), 1146–1149. https://doi.org/10.1161/01.cir.66.6.1146

Carmeliet, E. (1999). Cardiac ionic currents and acute ischemia: from channels to arrhythmias. *Physiological Reviews*, *79*(3), 917–1017. https://doi.org/10.1152/physrev.1999.79.3.917

Chen, R.-H., Li, Y.-G., Jiao, K.-L., Zhang, P.-P., Sun, Y., Zhang, L.-P., Fong, X.-F., Li, W., & Yu, Y. (2013). Overexpression of Sema3a in myocardial infarction border zone decreases vulnerability of ventricular tachycardia post-myocardial infarction in rats. *Journal of Cellular and Molecular Medicine*, *17*(5), 608–616. https://doi.org/10.1111/jcmm.12035

Chen, T., & Vunjak-Novakovic, G. (2019). Human Tissue-Engineered Model of Myocardial Ischemia-Reperfusion Injury. *Tissue Engineering. Part A*, *25*(9–10), 711–724. https://doi.org/10.1089/ten.TEA.2018.0212

de Jong, S., van Veen, T. A. B., van Rijen, H. V. M., & de Bakker, J. M. T. (2011). Fibrosis and cardiac arrhythmias. *Journal of Cardiovascular Pharmacology*, *57*(6), 630–638. https://doi.org/10.1097/FJC.0b013e318207a35f

Derrickson, B. H. , and G. J. T. (2021). *Principles of Anatomy & Physiology. 16th* (16th ed.).

Dun, W., Baba, S., Yagi, T., & Boyden, P. A. (2004). Dynamic remodeling of K+ and Ca2+ currents in cells that survived in the epicardial border zone of canine healed infarcted heart. *American Journal of Physiology. Heart and Circulatory Physiology*, *287*(3), H1046-54. https://doi.org/10.1152/ajpheart.00082.2004

Fearnley, C. J., Roderick, H. L., & Bootman, M. D. (2011). Calcium signaling in cardiac myocytes. *Cold Spring Harbor Perspectives in Biology*, *3*(11), a004242. https://doi.org/10.1101/cshperspect.a004242

Frampton, J., Ortengren, A. R., & Zeitler, E. P. (2023). Arrhythmias After Acute Myocardial Infarction. *The Yale Journal of Biology and Medicine*, *96*(1), 83–94. https://doi.org/10.59249/LSWK8578

Good, W. W., Zenger, B., Bergquist, J. A., Rupp, L. C., Gillette, K. K., Gsell, M. A. F., Plank, G., & MacLeod, R. S. (2021). Quantifying the spatiotemporal influence of acute myocardial ischemia on volumetric conduction velocity. *Journal of Electrocardiology*, *66*, 86–94. https://doi.org/10.1016/j.jelectrocard.2021.03.004

Häkli, M., Kreutzer, J., Mäki, A.-J., Välimäki, H., Cherian, R. M., Kallio, P., Aalto-Setälä, K., & Pekkanen-Mattila, M. (2022). Electrophysiological Changes of Human-Induced Pluripotent Stem Cell-Derived Cardiomyocytes during Acute Hypoxia and Reoxygenation. *Stem Cells International*, *2022*, 9438281. https://doi.org/10.1155/2022/9438281

Häkli, M., Kreutzer, J., Mäki, A.-J., Välimäki, H., Lappi, H., Huhtala, H., Kallio, P., Aalto-Setälä, K., & Pekkanen-Mattila, M. (2021). Human induced pluripotent stem cell-based platform for modeling cardiac ischemia. *Scientific Reports*, *11*(1), 4153. https://doi.org/10.1038/s41598-021-83740-w

Han, B., Trew, M. L., & Zgierski-Johnston, C. M. (2021). Cardiac Conduction Velocity, Remodeling and Arrhythmogenesis. *Cells*, *10*(11). https://doi.org/10.3390/cells10112923

Hegyi, B., Bossuyt, J., Griffiths, L. G., Shimkunas, R., Coulibaly, Z., Jian, Z., Grimsrud, K. N., Sondergaard, C. S., Ginsburg, K. S., Chiamvimonvat, N., Belardinelli, L., Varró, A., Papp, J. G., Pollesello, P., Levijoki, J., Izu, L. T., Boyd, W. D., Bányász, T., Bers, D. M., & Chen-Izu, Y. (2018). Complex electrophysiological remodeling in postinfarction ischemic heart failure. *Proceedings of the National Academy of Sciences of the United States of America*, *115*(13), E3036–E3044. https://doi.org/10.1073/pnas.1718211115

Hernández-Romero, I., Guillem, M. S., Figuera, C., Atienza, F., Fernández-Avilés, F., & M Climent, A. (2019). Optical imaging of voltage and calcium in isolated hearts: Linking spatiotemporal heterogeneities and ventricular fibrillation initiation. *PloS One*, *14*(5), e0215951. https://doi.org/10.1371/journal.pone.0215951

Hoeker, G. S., James, C. C., Tegge, A. N., Gourdie, R. G., Smyth, J. W., & Poelzing, S. (2020). Attenuating loss of cardiac conduction during no-flow ischemia through changes in perfusate sodium and calcium. *American Journal of Physiology-Heart and Circulatory Physiology*, *319*(2), H396–H409. https://doi.org/10.1152/ajpheart.00112.2020

Huikuri, H. V, Koistinen, M. J., Yli-Mäyry, S., Airaksinen, K. E., Seppänen, T., Ikäheimo, M. J., & Myerburg, R. J. (1995). Impaired low-frequency oscillations of heart rate in patients with prior acute myocardial infarction and life-threatening arrhythmias. *The American Journal of Cardiology*, *76*(1), 56–60. https://doi.org/10.1016/s0002-9149(99)80801-7

Jackson, B. M., Gorman, J. H., Moainie, S. L., Guy, T. S., Narula, N., Narula, J., John-Sutton, M. G., Edmunds, L. H., & Gorman, R. C. (2002). Extension of borderzone myocardium in postinfarction dilated cardiomyopathy. *Journal of the American College of Cardiology*, *40*(6), 1160–1167; discussion 1168-71. https://doi.org/10.1016/s0735-1097(02)02121-6

Jackson, B. M., Gorman, J. H., Salgo, I. S., Moainie, S. L., Plappert, T., St John-Sutton, M., Edmunds, L. H., & Gorman, R. C. (2003). Border zone geometry increases wall stress after myocardial infarction: contrast echocardiographic assessment. *American Journal of Physiology. Heart and Circulatory Physiology*, *284*(2), H475-9. https://doi.org/10.1152/ajpheart.00360.2002

Jenča, D., Melenovský, V., Stehlik, J., Staněk, V., Kettner, J., Kautzner, J., Adámková, V., & Wohlfahrt, P. (2021). Heart failure after myocardial infarction: incidence and predictors. *ESC Heart Failure*, *8*(1), 222–237. https://doi.org/10.1002/ehf2.13144

King, J. H., Huang, C. L.-H., & Fraser, J. A. (2013). Determinants of myocardial conduction velocity: implications for arrhythmogenesis. *Frontiers in Physiology*, *4*. https://doi.org/10.3389/fphys.2013.00154

Klabunde, R. E. (2017). Cardiac electrophysiology: normal and ischemic ionic currents and the ECG. *Advances in Physiology Education*, *41*(1), 29–37. https://doi.org/10.1152/advan.00105.2016

Kung, G. L., Vaseghi, M., Gahm, J. K., Shevtsov, J., Garfinkel, A., Shivkumar, K., & Ennis, D. B. (2018). Microstructural Infarct Border Zone Remodeling in the Post-infarct Swine Heart Measured by Diffusion Tensor MRI. *Frontiers in Physiology*, *9*, 826. https://doi.org/10.3389/fphys.2018.00826

Kuo, I. Y., & Ehrlich, B. E. (2015). Signaling in muscle contraction. *Cold Spring Harbor Perspectives in Biology*, *7*(2), a006023. https://doi.org/10.1101/cshperspect.a006023

Lau, D. H., Clausen, C., Sosunov, E. A., Shlapakova, I. N., Anyukhovsky, E. P., Danilo, P., Rosen, T. S., Kelly, C., Duffy, H. S., Szabolcs, M. J., Chen, M., Robinson, R. B., Lu, J., Kumari, S., Cohen, I. S., & Rosen, M. R. (2009). Epicardial border zone overexpression of skeletal muscle sodium channel SkM1 normalizes activation, preserves conduction, and suppresses ventricular arrhythmia: an in silico, in vivo, in vitro study. *Circulation*, *119*(1), 19–27. https://doi.org/10.1161/CIRCULATIONAHA.108.809301

Lindsey, M. L., Bolli, R., Canty, J. M., Du, X.-J., Frangogiannis, N. G., Frantz, S., Gourdie, R. G., Holmes, J. W., Jones, S. P., Kloner, R. A., Lefer, D. J., Liao, R., Murphy, E., Ping, P., Przyklenk, K., Recchia, F. A., Schwartz Longacre, L., Ripplinger, C. M., Van Eyk, J. E., & Heusch, G. (2018). Guidelines for experimental models of myocardial ischemia and infarction. *American Journal of Physiology. Heart and Circulatory Physiology*, *314*(4), H812–H838. https://doi.org/10.1152/ajpheart.00335.2017

Malakar, A. K., Choudhury, D., Halder, B., Paul, P., Uddin, A., & Chakraborty, S. (2019). A review on coronary artery disease, its risk factors, and therapeutics. *Journal of Cellular Physiology*, *234*(10), 16812–16823. https://doi.org/10.1002/jcp.28350

Mendonca Costa, C., Plank, G., Rinaldi, C. A., Niederer, S. A., & Bishop, M. J. (2018). Modeling the Electrophysiological Properties of the Infarct Border Zone. *Frontiers in Physiology*, *9*, 356. https://doi.org/10.3389/fphys.2018.00356

Mosterd, A., & Hoes, A. W. (2007). Clinical epidemiology of heart failure. *Heart (British Cardiac Society)*, *93*(9), 1137–1146. https://doi.org/10.1136/hrt.2003.025270

Mummery, C., Ward-van Oostwaard, D., Doevendans, P., Spijker, R., van den Brink, S., Hassink, R., van der Heyden, M., Opthof, T., Pera, M., de la Riviere, A. B., Passier, R., & Tertoolen, L. (2003). Differentiation of human embryonic stem cells to cardiomyocytes: role of coculture with visceral endoderm-like cells. *Circulation*, *107*(21), 2733–2740. https://doi.org/10.1161/01.CIR.0000068356.38592.68

Nargeot, J., Lory, P., & Richard, S. (1997). Molecular basis of the diversity of calcium channels in cardiovascular tissues. *European Heart Journal*, *18 Suppl A*, A15-26. https://doi.org/10.1093/eurheartj/18.suppl_a.15

Ng, F. S., Kalindjian, J. M., Cooper, S. A., Chowdhury, R. A., Patel, P. M., Dupont, E., Lyon, A. R., & Peters, N. S. (2016). Enhancement of Gap Junction Function During Acute Myocardial Infarction Modifies Healing and Reduces Late Ventricular Arrhythmia Susceptibility. *JACC. Clinical Electrophysiology*, *2*(5), 574–582. https://doi.org/10.1016/j.jacep.2016.03.007

Ojala, M., Rajala, K., Pekkanen-Mattila, M., Miettinen, M., Huhtala, H., & Aalto-Setälä, K. (2012). Culture conditions affect cardiac differentiation potential of human pluripotent stem cells. *PloS One*, *7*(10), e48659. https://doi.org/10.1371/journal.pone.0048659

Pekkanen-Mattila, M., Häkli, M., Pölönen, R.-P., Mansikkala, T., Junnila, A., Talvitie, E., Koivisto, J. T., Kellomäki, M., & Aalto-Setälä, K. (2019). Polyethylene Terephthalate Textiles Enhance the Structural Maturation of Human Induced Pluripotent Stem Cell-Derived Cardiomyocytes. *Materials (Basel, Switzerland)*, *12*(11). https://doi.org/10.3390/ma12111805

Piccini, J. P., Berger, J. S., & Brown, D. L. (2008). Early sustained ventricular arrhythmias complicating acute myocardial infarction. *The American Journal of Medicine*, *121*(9), 797–804. https://doi.org/10.1016/j.amjmed.2008.04.024

Prabhu, S. D., & Frangogiannis, N. G. (2016). The Biological Basis for Cardiac Repair After Myocardial Infarction: From Inflammation to Fibrosis. *Circulation Research*, *119*(1), 91–112. https://doi.org/10.1161/CIRCRESAHA.116.303577

Prajapati, C., Ojala, M., Lappi, H., Aalto-Setälä, K., & Pekkanen-Mattila, M. (2021). Electrophysiological evaluation of human induced pluripotent stem cell-derived cardiomyocytes obtained by different methods. *Stem Cell Research*, *51*, 102176. https://doi.org/10.1016/j.scr.2021.102176

Puymirat, E., Simon, T., Cayla, G., Cottin, Y., Elbaz, M., Coste, P., Lemesle, G., Motreff, P., Popovic, B., Khalife, K., Labèque, J.-N., Perret, T., Le Ray, C., Orion, L., Jouve, B., Blanchard, D., Peycher, P., Silvain, J., Steg, P. G., … USIK, U. 2000, and F.-M. investigators. (2017). Acute Myocardial Infarction: Changes in Patient Characteristics, Management, and 6-Month Outcomes Over a Period of 20 Years in the FAST-MI Program (French Registry of Acute ST-Elevation or Non-ST-Elevation Myocardial Infarction) 1995 to 2015. *Circulation*, *136*(20), 1908–1919. https://doi.org/10.1161/CIRCULATIONAHA.117.030798

Rexius-Hall, M. L., Khalil, N. N., Escopete, S. S., Li, X., Hu, J., Yuan, H., Parker, S. J., & McCain, M. L. (2022a). A myocardial infarct border-zone-on-a-chip demonstrates distinct regulation of cardiac tissue function by an oxygen gradient. *Science Advances*, *8*(49), eabn7097. https://doi.org/10.1126/sciadv.abn7097

Rexius-Hall, M. L., Khalil, N. N., Escopete, S. S., Li, X., Hu, J., Yuan, H., Parker, S. J., & McCain, M. L. (2022b). A myocardial infarct border-zone-on-a-chip demonstrates distinct regulation of cardiac tissue function by an oxygen gradient. *Science Advances*, *8*(49), eabn7097. https://doi.org/10.1126/sciadv.abn7097

Roger, V. L. (2013). Epidemiology of heart failure. *Circulation Research*, *113*(6), 646–659. https://doi.org/10.1161/CIRCRESAHA.113.300268

Rymer, J. A., Wegermann, Z. K., Wang, T. Y., Li, S., Smilowitz, N. R., Wilson, B. H., Jneid, H., & Tamis-Holland, J. E. (2024). Ventricular Arrhythmias After Primary Percutaneous Coronary Intervention for STEMI. *JAMA Network Open*, *7*(5), e2410288. https://doi.org/10.1001/jamanetworkopen.2024.10288

Schelbert, E. B., Hsu, L.-Y., Anderson, S. A., Mohanty, B. D., Karim, S. M., Kellman, P., Aletras, A. H., & Arai, A. E. (2010). Late gadolinium-enhancement cardiac magnetic resonance identifies postinfarction myocardial fibrosis and the border zone at the near cellular level in ex vivo rat heart. *Circulation. Cardiovascular Imaging*, *3*(6), 743–752. https://doi.org/10.1161/CIRCIMAGING.108.835793

Schmidt, A., Azevedo, C. F., Cheng, A., Gupta, S. N., Bluemke, D. A., Foo, T. K., Gerstenblith, G., Weiss, R. G., Marbán, E., Tomaselli, G. F., Lima, J. A. C., & Wu, K. C. (2007). Infarct tissue heterogeneity by magnetic resonance imaging identifies enhanced cardiac arrhythmia

susceptibility in patients with left ventricular dysfunction. *Circulation*, *115*(15), 2006–2014. https://doi.org/10.1161/CIRCULATIONAHA.106.653568

Sinnenberg, L., & Givertz, M. M. (2020). Acute heart failure. *Trends in Cardiovascular Medicine*, *30*(2), 104–112. https://doi.org/10.1016/j.tcm.2019.03.007

Spaulding, K., Takaba, K., Collins, A., Faraji, F., Wang, G., Aguayo, E., Ge, L., Saloner, D., Wallace, A. W., Baker, A. J., Lovett, D. H., & Ratcliffe, M. B. (2018). Short term doxycycline treatment induces sustained improvement in myocardial infarction border zone contractility. *PloS One*, *13*(2), e0192720. https://doi.org/10.1371/journal.pone.0192720

St John Sutton, M., Lee, D., Rouleau, J. L., Goldman, S., Plappert, T., Braunwald, E., & Pfeffer, M. A. (2003). Left ventricular remodeling and ventricular arrhythmias after myocardial infarction. *Circulation*, *107*(20), 2577–2582. https://doi.org/10.1161/01.CIR.0000070420.51787.A8

Thygesen, K., Alpert, J. S., Jaffe, A. S., Simoons, M. L., Chaitman, B. R., White, H. D., Writing Group on the Joint ESC/ACCF/AHA/WHF Task Force for the Universal Definition of Myocardial Infarction, Thygesen, K., Alpert, J. S., White, H. D., Jaffe, A. S., Katus, H. A., Apple, F. S., Lindahl, B., Morrow, D. A., Chaitman, B. A., Clemmensen, P. M., Johanson, P., Hod, H., … ESC Committee for Practice Guidelines (CPG). (2012). Third universal definition of myocardial infarction. *European Heart Journal*, *33*(20), 2551–2567. https://doi.org/10.1093/eurheartj/ehs184

Tran, D. B., Weber, C., & Lopez, R. A. (2024). *Anatomy, Thorax, Heart Muscles*.

Trew, M. L., Engelman, Z. J., Caldwell, B. J., Lever, N. A., LeGrice, I. J., & Smaill, B. H. (2019). Cardiac intramural electrical mapping reveals focal delays but no conduction velocity slowing in the peri-infarct region. *American Journal of Physiology. Heart and Circulatory Physiology*, *317*(4), H743–H753. https://doi.org/10.1152/ajpheart.00154.2019

Wan Ab Naim, W. N., Mokhtarudin, M. J. M., Lim, E., Chan, B. T., Ahmad Bakir, A., & Nik Mohamed, N. A. (2020). The study of border zone formation in ischemic heart using electro-chemical coupled computational model. *International Journal for Numerical Methods in Biomedical Engineering*, *36*(11), e3398. https://doi.org/10.1002/cnm.3398

Wei, X., Yohannan, S., & Richards, J. R. (2024). *Physiology, Cardiac Repolarization Dispersion and Reserve*.

Weigand, K., Witte, R., Moukabary, T., Chinyere, I., Lancaster, J., Pierce, M. K., Goldman, S., & Juneman, E. (2017). In vivo Electrophysiological Study of Induced Ventricular Tachycardia in Intact Rat Model of Chronic Ischemic Heart Failure. *IEEE Transactions on Bio-Medical Engineering*, *64*(6), 1393–1399. https://doi.org/10.1109/TBME.2016.2605578

Wong, D. T. L., Weightman, M. J., Baumert, M., Tayeb, H., Richardson, J. D., Puri, R., Bertaso, A. G., Roberts-Thomson, K. C., Sanders, P., Worthley, M. I., & Worthley, S. G. (2012). Electro-mechanical characteristics of myocardial infarction border zones and ventricular arrhythmic risk: novel insights from grid-tagged cardiac magnetic resonance imaging. *European Radiology*, *22*(8), 1651–1658. https://doi.org/10.1007/s00330-012-2417-2